JOURNAL OF PETROLOGY | VOLUME 45 | NUMBER 8 | PAGES 1583–1612 | 2004 | DOI: 10.1093/petrology/egh024

Hf Isotope Systematics of Kimberlites and their Megacrysts: New Constraints on their Source Regions

G. M. NOWELL[1]*, D. G. PEARSON[1], D. R. BELL[2], R. W. CARLSON[3], C. B. SMITH[4], P. D. KEMPTON[5] AND S. R. NOBLE[5]

[1]ARTHUR HOLMES ISOTOPE GEOLOGY LABORATORY, DEPARTMENT OF EARTH SCIENCES, DURHAM UNIVERSITY, SOUTH ROAD, DURHAM DH1 3LE, UK

[2]ARIZONA STATE UNIVERSITY, CHEMISTRY AND BIOLOGY, PO BOX 871604, TEMPE, AZ 85287, USA

[3]CARNEGIE INSTITUTION OF WASHINGTON, 5241 BROAD BRANCH ROAD NW, WASHINGTON, DC 20015, USA

[4]DEBEERS CONSOLIDATED MINES, GEOSCIENCE CENTRE, PO BOX 82232, SOUTHDALE GAUTENG 2135, SOUTH AFRICA

[5]NERC ISOTOPE GEOSCIENCES LABORATORY, KINGSLEY DUNHAM CENTRE, KEYWORTH, NOTTINGHAM NG12 5HH, UK

RECEIVED MAY 20, 2001; ACCEPTED FEBRUARY 2, 2004
ADVANCE ACCESS PUBLICATION JULY 1, 2004

Kimberlites from Southern Africa, along with their low-Cr megacrysts, have unusual Hf–Nd isotopic characteristics. Group I and Transitional kimberlites define arrays trending oblique to, and well below, the Nd–Hf isotope 'mantle array', defined by oceanic basalts, i.e. they have negative $\Delta\varepsilon_{Hf}$ *values. Group I kimberlites have* $\Delta\varepsilon_{Hf}$ *values varying from −1.2 to −10.1. Low-Cr megacryst suites from individual Group I kimberlites have compositions that overlap those of their host kimberlites. The trend for all Group I kimberlite megacrysts (*$\Delta\varepsilon_{Hf}$ *values −1.0 to −9.0) shows a striking correspondence to that of the Group I kimberlite field. Group II kimberlites and their low-Cr megacrysts plot on or close to the mantle Nd–Hf array (*$\Delta\varepsilon_{Hf}$ *values 3.6 to −2.6). The data indicate a genetic link between kimberlites and the low-Cr megacryst suite. The negative* $\Delta\varepsilon_{Hf}$ *characteristics of Group I kimberlites and their megacrysts require a source component that is ancient (> 1 Ga), and has evolved with low time-integrated Lu/Hf relative to Sm/Nd. Our preferred option is that this component originates beneath the lithosphere, from a reservoir of ancient, deeply subducted oceanic basalt that became incorporated into the convecting mantle source region for Group I and Transitional kimberlites.*

KEY WORDS: *isotopes; kimberlites; lutetium–hafnium; megacrysts*

INTRODUCTION

Despite the mineralogical sensitivity of the Lu–Hf isotope system to fractionation (Fig. 1), the vast majority of mantle and crustal rocks analysed so far lie along a single, well-correlated array in Hf–Nd isotope space. Lithologies as diverse as mid-ocean ridge basalts, ocean island basalts, island arc volcanics and upper crust of various ages lie on, or close to, this array (see Blichert-Toft, 2001 for a review), suggesting similar, coupled fractionation of Sm/Nd and Lu/Hf in most terrestrial magma source reservoirs. Kimberlites are deeply derived volcanic ocks, for which a great diversity of different source regions and components have been advocated, ranging from continental lithospheric mantle (CLM), convecting upper mantle, subducted oceanic crust and the lower mantle or core–mantle boundary (e.g. Sharp, 1974; Smith, 1983; le Roux, 1986; Mitchell, 1986; Haggerty, 1994; Kesson *et al.*, 1994). They are also the only rock type to contain samples of both upper and lower mantle (Harte, 1999). The possible ultra-deep origins of kimberlites combined with the wide variation in Lu/Hf fractionation through this depth interval (Fig. 1) suggest the possibility of finding distinctive Nd–Hf isotopic compositions in these rocks. In particular, the

*Corresponding author. Telephone: +44 (0) 191 3342339; Fax: +44 (0) 191 3342301. E-mail: g.m.nowell@durham.ac.uk

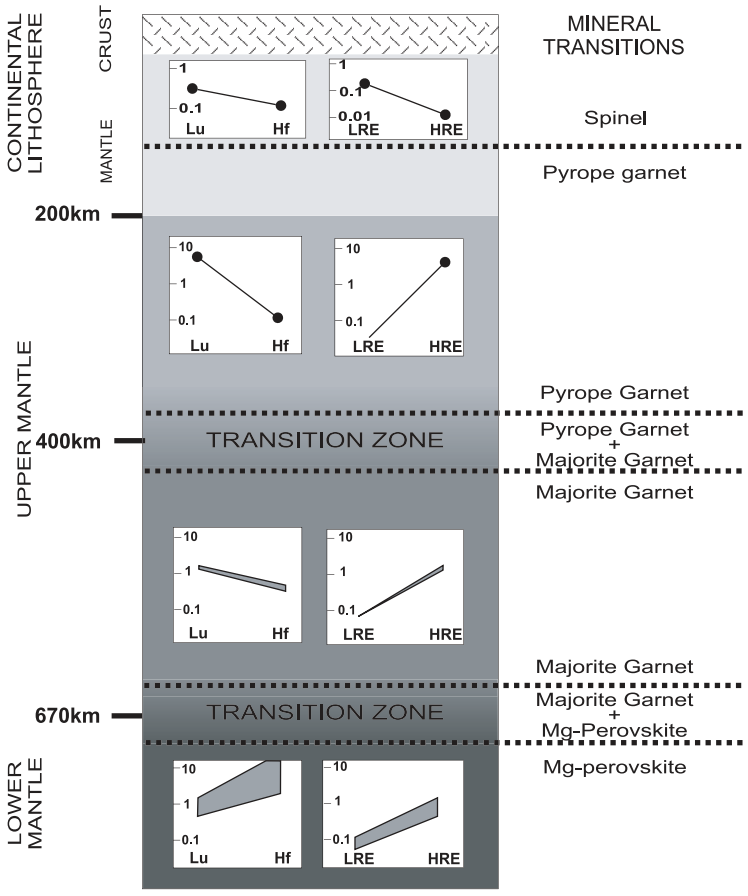

Fig. 1. Schematic cross-section through the Earth's crust and mantle, showing the major mineral transitions of importance to the Lu–Hf isotope system. The range of distribution coefficients for Lu, Hf, Sm and Nd is shown for each of the mineral phases in the zones shown. LRE, Light rare earth elements; HRE, heavy rare earth elments.

characteristic Lu/Hf–Sm/Nd fractionation systematics of ultra-deep phases such as majorite and perovskite (Fig. 1) compared with shallower phases could be discernible.

The study of Nowell *et al.* (1999) established that kimberlites have distinctive Hf–Nd isotope systematics that plot off the mantle array. Lamproites also have anomalous Hf–Nd isotope systematics that plot well below the mantle array (Nowell *et al.*, 1998*a*, 1999), indicating the presence of a distinctive mantle reservoir in these rocks. In addition, Janney *et al.* (2002) have found similar signatures in mafic alkalic/potassic rocks surrounding the Kaapvaal craton and even into the southern Atlantic Ocean (Alphard Bank). Here, we analyse a more extensive kimberlite sample set, to explore further the implications for kimberlite source regions and deep mantle reservoirs. Low-Cr megacrysts from eight kimberlites have also been analysed, to try to further constrain the relationships between megacrysts and kimberlites and to examine in more detail the source contributions to kimberlite-related magmatism.

The unusual Hf–Nd isotope characteristics of the kimberlite–megacryst magma source region also provide constraints relevant to terrestrial geochemistry mass balance arguments. Mixing between bulk crust and depleted mantle do not intersect most estimates of Bulk Silicate Earth (BSE) based on meteorites (e.g. Blichert-Toft & Albarede, 1997) and this mass balance problem has been interpreted to indicate the existence of a reservoir that is not sampled by terrestrial rocks (Blichert-Toft & Albarede, 1997). Our new data confirm earlier findings (Nowell *et al.*, 1998*b*; Pearson & Nowell, 2002) that kimberlites and their megacrysts have Hf–Nd isotope systematics that are suitable for the 'missing reservoir', or at least point to the existence of such a reservoir.

SAMPLES

Kimberlites

Kimberlites are a mixture of components that are derived from every 'reservoir' through which they have ascended en route to the surface. This greatly complicates the interpretation of their elemental and isotopic signatures. These problems cannot be eradicated with certainty in

any study of kimberlite whole-rock geochemistry, but, to minimize any such difficulties, our samples were chosen from previously characterized, fresh, hypabyssal-facies kimberlites, specifically selected for their minimal crustal contamination (Smith, 1983; Smith *et al.*, 1985; McDonald *et al.*, 1995). The samples studied are from Southern Africa, belonging to the isotopic Groups I and II of Smith (1983), or kimberlites and 'orangeites' as classified by Mitchell (1995), along with Transitional kimberlites (Skinner *et al.*, 1994) that have Sr and Nd isotope characteristics intermediate to Group I and Group II kimberlites. For sample descriptions and major element compositions, the reader is referred to the appendices of Smith *et al.* (1985), Fraser & Hawkesworth (1992) and McDonald *et al.* (1995).

Megacrysts

Kimberlites commonly contain large (1–20 cm) single silicate and oxide phases of a distinctive Cr-poor, Ti-rich character, commonly referred to as 'discrete nodules' (Nixon & Boyd, 1973) or 'Cr-poor megacrysts' (Eggler *et al.*, 1979). In Group I kimberlites, the Cr-poor megacryst assemblage includes Cr-poor pyrope garnet, clinopyroxene, orthopyroxene, phlogopite, magnesian ilmenite, zircon and Fe-rich olivine, whereas, in Group II kimberlites, only garnet and, occasionally, clinopyroxene are present (Moore *et al.*, 1992; Bell *et al.*, 1995). The origin of megacrysts and the relationship between megacrysts and their host kimberlites is certainly not fully resolved. However, petrological and geochemical evidence indicates that the megacrysts in Group I kimberlites formed from an alkali-basalt-like magma that was probably the precursor to, or intimately related to, the host kimberlite. In many cases, this magma crystallized in the lower parts of the lithospheric mantle, probably close to the lithosphere–asthenosphere boundary (Harte & Gurney, 1981; Mitchell, 1986; Hops *et al.*, 1992). Past estimates of the REE composition of this parental magma (La/Yb_n ~20) tend to be more Ocean-Iland Basalt (OIB) like than kimberlitic in character, suggesting derivation from the sublithospheric mantle (Harte, 1983; Jones, 1987; Davies *et al.*, 2001) and this is also supported by the OIB-like Sr–Nd–Pb isotope data (Smith *et al.*, 1985; Jones, 1987; Spriggs, 1988; Hops *et al.*, 1992; Davies *et al.*, 2001). The REE data, combined with subtle differences in isotopic composition between megacrysts and kimberlites, have been used to argue against a close genetic relationship (Jones, 1987; Davies *et al.*, 2001). However, as pointed by Davies *et al.* (2001), few isotopic studies, including their own, have actually compared megacryst isotopic compositions directly with their host kimberlite.

We have analysed the Nd and Hf isotope composition of both megacrysts and their host kimberlite from the Premier, Monastery, Jagersfontein, Gansfontein and Frank Smith Group I kimberlites. In addition, megacrysts, but not the host kimberlite from the Thaba Putsoa, Letseng, Kao, Mothae (all Lesotho), Orapa (Botswana), Kallvallei and Star (S. Africa) kimberlites plus the Kamfersdam dump (Kimberley, S. Africa) have been analysed. Zircon megacrysts from these localities have only been analysed for Hf isotope composition. The Monastery megacryst suite is one of the most extensively studied and comprises garnets, phlogopites, clinopyroxenes, clinopyroxenes–ilmenite intergrowths, ilmenites, zircon–ilmenite intergrowths and zircons (Gurney *et al.*, 1979).

SAMPLE PREPARATION AND ANALYTICAL TECHNIQUES

New kimberlite samples prepared for this study were carefully hand-picked to screen out crustal fragments, altered grains and obvious megacryst and xenolith-related grains. Every precaution was taken during picking and preparation of the megacrysts to avoid inclusions, grain-boundary alteration and areas with signs of host–kimberlite interaction. The ilmenite samples analysed were either part of bi-mineralic intergrowths with zircon, or large (cm or greater), deformation-free monocrystals. The outer edges and surfaces of all the megacrysts were removed before being lightly crushed (<2 mm Ø) for picking. Garnets and clinopyroxenes were picked under ethanol and only clear translucent fragments were selected. As the ilmenites are opaque, only those fragments with good conchoidal fractures were picked. After the first picking, all the megacrysts were washed in 18.2 MΩ water and ultrasonically leached in 6 N HCl for 30 minutes before being washed with 18.2 MΩ water a second time, crushed to a finer size and re-picked. After this second picking, the acid leach and wash steps were repeated before the samples were powdered. Although no inclusions were observed within any of the megacrysts during this process, it is possible that very small inclusions have been overlooked and the possibility exists for some of the ilmenites with very low Nd contents to have been influenced by inclusions of more REE-rich minerals. These effects are minor and do not alter our conclusions.

All kimberlite and megacryst samples, except zircons, were analysed for trace element and rare earth element compositions at Durham University using an Elan 6000 ICP-MS. Sample dissolution and ICP-MS analytical protocols have been presented by Ottley *et al.* (2003). Instrument calibration is made using international rock standards. Internal spikes are used to monitor suppression and drift. The reproducibility (relative standard deviation) of the in-house kimberlite standard using these techniques is 2.4% for Lu/Hf ratios and 1.1% for Sm/Nd ratios. Mineral separate analyses using longer on-peak dwell times give data that are a factor of two better than this.

Sr, Nd and Hf isotopic compositions were determined at three different laboratories: NERC Isotope Geosciences Laboratory (NIGL; see Nowell *et al.*, 1998*c*; Royse *et al.*, 1998; Nowell & Parrish, 2001 for relevant analytical protocols), the Department of Terrestrial Magmatism (DTM; see Carlson & Nowell, 2001 for analytical protocols) and, latterly, at the Arthur Holmes Isotope Geology Laboratory, Durham University (AHIGL; see Nowell *et al.*, 2003*a* for analytical protocols). The Hf separation procedure adopted for samples analysed by plasma ionization multi-collector mass spectrometry (PIMMS) required only the first two anion exchange columns described by Nowell *et al.* (1998) to remove the bulk of the sample and titanium, respectively. The Hf–Nd separation procedure used at Durham has been documented by Dowall *et al.* (2003). Data were collected by a combination of TIMS and PIMMS over several analytical sessions. Details relating to standard normalization, precision and accuracy and constants used are given in the legends to Tables 1–3.

RESULTS

Although many of the kimberlites in Table 1 have been previously characterized for Nd and Sr isotopes (Smith, 1983; Skinner *et al.*, 1994), we have re-analysed the majority of samples to maintain an internally consistent database and to improve upon precision. All plotted kimberlite and megacryst data are initial values, calculated using the kimberlite eruption ages and the relevant parameters given in Table 1.

Group I kimberlites

On a Nd–Sr isotope diagram (Fig. 2), Cretaceous Southern African Group I kimberlites plot as a field within the mantle array characterized by Sr isotope compositions close to Bulk Earth (BE) and generally positive ε_{Ndi} values (−0.5 to 4.0). This field is distinct from Southern African Cretaceous Group II kimberlites that have more radiogenic Sr isotope and less radiogenic Nd isotope compositions (Smith, 1983). In ε_{Hfi}–ε_{Ndi} space (Fig. 3a), the Group I kimberlite field ranges from compositions that have both positive and negative ε_{Hfi} values (−6.2 to +7.3) and generally positive ε_{Ndi}. Two samples have both negative ε_{Hfi} and ε_{Ndi}. The data do not plot along the oceanic array but are displaced below it to varying degrees. The departure of Group I kimberlites from the main oceanic array can be expressed using the $\Delta\varepsilon_{Hf}$ notation (Table 1) of Johnson & Beard (1993). We use the revised regression of the oceanic array of Vervoort *et al.* (1999). Samples that plot above the array have positive $\Delta\varepsilon_{Hf}$ and those that plot below the array have negative $\Delta\varepsilon_{Hf}$. Without exception, Southern African Group I kimberlites are characterized by negative $\Delta\varepsilon_{Hf}$ values (−1.2 to −10.1; Figs 4a and 5). There is no clear systematic variation of $\Delta\varepsilon_{Hf}$ with ε_{Nd}. This strongly negative $\Delta\varepsilon_{Hf}$ isotope signature is not observed in volcanic rocks from the ocean basins, with the exception of a slightly less pronounced negative signature in HIMU OIBs (Figs 4a and 5; Ballentine *et al.*, 1997). Kimberlites, along with lamproites (Nowell *et al.*, 1998*b*), record the largest displacements below the mantle Hf–Nd array yet measured in mantle-derived volcanic rocks.

Group II kimberlites

Group II kimberlites have unradiogenic Nd (ε_{Ndi} −5.5 to −11.9) coupled with radiogenic Sr isotope compositions (0.7078–0.7126), plotting in the 'enriched' quadrant of the Nd–Sr isotope diagram (Fig. 2a; Smith, 1983). Hf isotope compositions are also unradiogenic (ε_{Hfi} −3.6 to −23.9), consistent with their trace element-enriched character. Although Nd isotope compositions of Group II kimberlites are distinct from those of Group I, their Hf isotope compositions partially overlap (Fig. 3a). Three-quarters of the Group II kimberlites analysed scatter around the mantle regression line of Vervoort *et al.* (1999), with $\Delta\varepsilon_{Hf}$ values between 2.4 and −2.6 (Fig. 5). However, two Group II kimberlites from Swartruggens plot well below the mantle regression line ($\Delta\varepsilon_{Hf}$ −8.7 to −12; Fig. 5).

Transitional kimberlites

'Transitional' kimberlites have Sr–Nd isotope compositions (Fig. 2a) that are intermediate between those of Group I and Group II. These kimberlites have less radiogenic Nd isotope compositions than Group I kimberlites—more characteristic of the so-called EMI mantle end-member. In addition to Southern African variants (Skinner *et al.*, 1994; Table 1), kimberlites with these isotopic compositions have also been reported from Brazil (Bizzi *et al.*, 1994; Carlson *et al.*, 1996), from the Arkhangelsk Region of Russia (Beard *et al.*, 2000; Mahotkin *et al.*, 2000) and from the North West Territories (Dowall *et al.*, 2000). Despite having ε_{Hfi} values that appear more similar to Group II kimberlites, Transitional kimberlites appear to lie on an extension of the Group I kimberlite array in ε_{Hfi}–ε_{Ndi} space (Fig. 3a), displaced well below the mantle array ($\Delta\varepsilon_{Hf}$ −8.1 to −14.2; Fig. 4a).

Kimberlite megacrysts

As observed in previous studies (Kramers *et al.*, 1981; Jones, 1987; Davies *et al.*, 2001), Nd–Sr isotope systematics of low-Cr megacrysts from Group I kimberlites are similar, but not exactly the same as their hosts (Fig. 2b). Excepting one sample, the range in Nd isotope compositions is comparable but the megacrysts have Sr isotope compositions at the least radiogenic end of the range shown by kimberlites. The low-Cr megacrysts from Group II kimberlites analysed here (Fig. 2b) and by Smith

Table 1: Hf–Nd–Sr isotope data for Group I and Group II kimberlites from Southern Africa

Kimberlite	Sample number	Loc w.r.t. craton	Age (Ma)	Lu	Hf	$^{176}Lu/^{177}Hf$	$^{176}Hf/^{177}Hf_n$	ε_{Hfi}	$\Delta\varepsilon_{Hf}$	Sm	Nd	$^{143}Nd/^{144}Nd_n$	ε_{Ndi}	Rb	Sr	$^{87}Sr/^{86}Sr_n$
Group I kimberlites																
Premier (SA)	P-Piebald	ON	1180	0·21	6·4	0·0047	0·282034 (14)[3]	−3·4	−10·1	19·2	123·35	0·511985 (6)[a]	2·7	3	1125	0·703529 (10)[a]
Premier (SA)	P-Carbonatite	ON	1180	0·21	6·43	0·0047	0·282192 (10)[3]	2·22								
Schuller (SA)	CBS 1087-4	ON	1180	0·08	2·71	0·0042	0·282057 (10)[3]	−2·2	−8·4	9·3	64·7	0·511903 (6)[a]	2·2	1·5	38·9	0·707188 (12)[a]
Schuller (SA)	CBS 1087-4rpt	ON	1180	0·08	2·71	0·0042	0·282076 (8)[3]	−1·5	−7·7	9·3						
Frank Smith (SA)	FS-K1	ON	114	0·09	4·76	0·0027	0·282592 (52)[1]	−40	−7·9	14·8	111·5	0·512582 (6)[a]	0·6	27·5	715·5	0·704762 (12)[a]
Frank Smith (SA)	FSM-2	ON	114	0·22	2·72	0·0115	0·282625 (7)[5]	−3·5	−6·1	5·6	36	0·512536 (11)[c]	−0·5	64·2	764	0·708046 (13)[c]
Monastery (SA)	MON-1	ON	90	0·11	12·11	0·0013	0·282764 (20)[1]	1·7	−5·2	12·3	83·2	0·512719 (6)[a]	2·8	79	652·2	0·704551 (10)[a]
Monastery (SA)	MON-1rpt	ON	90	0·11	12·11	0·0013	0·282730 (20)[3]	0·5	−6·4							
Monastery (SA)	MON GREEN	ON	90	0·1	13·05	0·0011	0·282698 (19)[3]	−0·6	−7·1	12·3	78·5	0·512707 (6)[a]	2·5	77	665	0·704572 (10)[a]
Jagersfontein (SA)	JAG K9	ON	86	0·06	2·9	0·0029	0·282805 (24)[1]	3	−2·9	52·5	407·4	0·512675 (8)[a]	2	141	247	0·706138 (10)[a]
Jagersfontein (SA)	JAG K9rpt	ON	86	0·06	2·9	0·0029	0·282826 (29)[3]	3·8	−2·1	52·5	407·4	0·512673 (8)[a]	2	141	247	0·706138 (10)[a]
Jagersfontein (SA)	PHN 2811	ON	86	0·04	0·82	0·007	0·282552 (24)[1]	−6·2	−9·2	1·4	8·9	0·512573 (7)[a]	−0·1	31·2	189·8	0·705979 (12)[a]
Jagersfontein (SA)	PHN 2811rpt	ON	86	0·04	0·82	0·007	0·282581 (15)[3]	−5·2	−8·1							
Jagersfontein (SA)	JAG 46	ON	86	0·08	5·6	0·002	0·282771 (19)[3]	1·9								
Benfontein (SA)	BEN-1	ON	90	0·16	21·5	0·0011	0·282758 (8)[2]	1·5	−4·4	43·6	333·2	0·512675 (8)[a]	2	5·1	917·9	0·705105 (10)[a]
Kaalvallie (SA)	KAA-1	ON	85	0·14	11·16	0·0018	0·282724 (9)[3]	0·2	−6·5	16·7	108·6	0·512714 (8)[a]	2·6	79·9	749·7	0·703768 (12)[a]
Wesselton (SA)	Wess 423	ON	86	0·08	4·53	0·0025	0·282600 (37)[3]	−4·2	−9·8	8·4	58	0·512668 (6)[a]	1·8	102·7	938·2	0·704191 (10)[a]
Liqhobong	LQ-7	ON	90	0·16	5·16	0·0044	0·282742 (9)[4]	0·8	−5·4	12	80	0·512692 (8)[b]	2·3	102·9	937	0·704005 (8)[b]
Pipe 200	P200	ON	90	0·1	9·3	0·0015	0·282740 (5)[5]	0·9	−7·3	11	74	0·512768 (7)[c]	3·8	80·3	745	0·703550 (9)[c]
Pampoenport (SA)	27/K16/6	OFF	103	0·09	5·71	0·0022	0·282713 (15)[3]	0·1	−4·1	12·3	90	0·512602[d]	0·8	55·5	861	0·70493[d]
Gansfontein	GNS-13	OFF	100	0·22	54·5	0·0006	0·282708 (5)[4]	0	−7·7	28·9	198	0·512742 (10)[b]	3·4	82·9	1687	0·704081 (12)[b]
Violkraal (SA)	26/K46/3	OFF	90	0·39	11·02	0·005	0·282713 (13)[3]	−0·6	−7·5	41·4	258·7	0·512732[d]	2·8	38	1565	0·70357[d]
Hartbeesfontein (SA)	27/K1/16	OFF	74	0·17	7·8	0·0031	0·282836 (29)[3]	3·9	−3·7	12·2	73·5	0·512761 (6)[a]	3·3	128·8	1178·2	0·704006 (12)[a]
Britstown (SA))	26/K35	OFF	74	0·16	7·6	0·0023	0·282761 (6)[3]	1·2	−5·7	16·3	105·9	0·512732[d]	2·8	69·6	1051·7	–
Gibeon (NAM)	33/K5	OFF	71·5	0·09	6·58	0·0019	0·282933 (28)[1]	7·3	−1·2	10·7	77·3	0·512791 (7)[a]	4	18·4	881·1	0·704376 (10)[a]
GROUP II kimberlites																
Swartruggens (SA)	Main 14/6	ON	145	0.28	12.57	0.0032	0.282013 (30)[1]	−23.9	−12	23.7	190.1	0.511944 (8)[a]	−11.3	271.2	1248.8	0.709947 (10)[a]
Swartruggens (SA)	Main 15/1	ON	145	0.28	12.77	0.0031	0.282088 (10)[1]	−21.2	−8.7	25.2	199.8	0.511920 (6)[a]	−11.8	242.7	814.5	0.712628 (12)[a]
Roberts Victor	PHN2386	ON	127	0.34	13.3	0.0036	0.282289 (8)[3]	−14.5	−1.9	20	173.5	0.511925 (8)[a]	−11.9	81.6	2034	0.708157 (10)[a]
Roberts Victor	ROVIC-1	ON	127	0.33	13.52	0.0034	0.282283 (7)[4]	−14.7	−2.6	33.4	311	0.511940 (6)[b]	−11.5	75.8	2036	0.707729 (8)[b]
Finsch (SA)	F445	ON	118	0.05	2.94	0.0024	0.282578 (12)[1]	−4.3	0.7	4.7	38.1	0.512226 (8)[a]	−6.2	154.2	562.9	0.710011 (10)[a]
Finsch (SA)	F756	ON	118	0.12	8.21	0.0021	0.282468 (29)[3]	−8.2	−0.6	12.6	96.5	0.512129 (6)[a]	−8.1	204.6	996.2	0.709922 (12)[a]
Finsch (SA)	F757	ON	118	0.1	5.72	0.0025	0.282593 (12)[3]	−3.8	0.3	0.8	80	0.512209 (6)[a]	−5.5	170.3	871.1	0.709714 (10)[a]

Table 1: Continued

Kimberlite	Sample number	Loc w.r.t. craton	Age (Ma)	Lu	Hf	$^{176}Lu/^{177}Hf$	$^{176}Hf/^{177}Hf_n$	ε_{Hfi}	$\Delta\varepsilon_{Hf}$	Sm	Nd	$^{143}Nd/^{144}Nd_n$	ε_{Ndi}	Rb	Sr	$^{87}Sr/^{86}Sr_n$
Finsch (SA)	F767	ON	118	0.03	3.01	0.0014	0.282595 (15)[3]	−3.7	2.3	5.1	39	0.512193 (8)[a]	−6.9	138	531.5	0.710199 (12)[a]
LACE (SA)	LACE3	ON	133	0.14	8.51	0.0023	0.282579 (8)[1]	−3.8	2.4	14.5	115.8	0.512162 (6)[a]	−7.1	169.5	1416.4	0.707879 (10)[a]
LACE (SA)	LACE3rpt	ON	133	0.14	8.51	0.0023	0.282569 (8)[3]	−4.2	2							
Bellsbank (SA)	FRB 430M	ON	120	0.16	5.4	0.0042	0.282370 (23)[3]	−11.8	−2.9	17.7	177	0.512067 (8)[a]	−9.1	103.7	1460.4	0.708275 (14)[a]
Newlands (SA)	PHN 2800	ON	120	0.16	3.68	0.0062	0.282393 (15)[3]	−11.1	−2	—	—	—	—	—	—	—
Slypsteen (SA)	26/K24/5	OFF	120	0.14	7.5	0.0027	0.282330 (11)[3]	−13.1	−1.1	12.8	97.7	0.511992[d]	−11.5	160.2	1174.8	0.70908[d]
Transitional kimberlites																
Melton Wold (SA)	27/K9	ON	145	0.08	1.97	0.0058	0.282405 (7)[3]	−10.2	−10	8.2	66.2	0.512389 (8)[a]	−2.6	95.7	815.18	0.707091 (10)[a]
Melton Wold (SA)	MW-3	ON	145	0.11	3.69	0.0043	0.282463 (16)[4]	−8	−8.1	7.8	62	0.512404 (10)[b]	−2.3	144.7	1147	0.706953 (10)[b]
Droogfontein (SA)	27/K19/2	ON	175	0.19	10.69	0.0025	0.282166 (14)[3]	−17.7	−14.2	14.1	100.8	0.512292[d]	−4.2	111.1	1683	0.70706[d]

All sample data are normalized relative to the following accepted or recommended standard values, Hf: $^{176}Hf/^{177}Hf$ ratio of 0.28216 for JMC 475 (Blichert-Toft *et al.*, 1997; Nowell *et al.*, 1998); Nd: $^{143}Nd/^{144}Nd$ ratios for La Jolla of 0.51186 and for J&M of 0.511110 (equivalent to the accepted La Jolla value); Sr: $^{87}Sr/^{86}Sr$ ratio for NBS 987 of 0.71024 (Thirlwall, 1991). All internal errors are 2SE.

Hf isotope compositions were determined by a combination of TIMS and PIMMS over several analytical sessions. Method of analysis, together with the average $^{176}Hf/^{177}Hf$ ratio and external reproducibility for JMC 475 for individual samples, are indicated by the superscript numbers in the $^{176}Hf/^{177}Hf_n$ column.

[1]TIMS analysis (MAT 262). Average $^{176}Hf/^{177}Hf$ ratio and external reproducibility for JMC 475 was 0.282155 ± 18 2SD ($n = 50$).

[2]TIMS analysis (MAT 262). Average $^{176}Hf/^{177}Hf$ ratio and external reproducibility for JMC 475 was 0.282160 ± 9 2SD ($n = 21$).

[3]PIMMS analysis (P54). Average $^{176}Hf/^{177}Hf$ ratio and external reproducibility for JMC 475 was 0.282105 ± 31 2SD ($n = 21$).

[4]PIMMS analysis (P54). Average $^{176}Hf/^{177}Hf$ ratio and external reproducibility for JMC 475 was 0.282178 ± 12 2SD ($n = 12$).

[5]PIMMS analysis (ThermoFinnigan Neptune). Average $^{176}Hf/^{177}Hf$ ratio and external reproducibility for JMC 475 was 0.282163 ± 5 2SD ($n = 12$).

Nd and Sr isotope data were collected over three analytical sessions or are taken from the literature, as indicated by the superscript letters.

[a]TIMS (MAT 262) analysis. Average $^{143}Nd/^{144}Nd$ and $^{87}Sr/^{86}Sr$ ratios for La Jolla and NBS 987 during the period of analysis were 0.511877 ± 18 2SD ($n = 33$) and 0.710195 ± 30 2SD ($n = 25$), respectively.

[b]TIMS (MAT 262) analysis. Average $^{143}Nd/^{144}Nd$ and $^{87}Sr/^{86}Sr$ ratios for La Jolla and NBS 987 during the period of analysis were 0.511931 ± 21 2SD ($n = 8$) and 0.710263 ± 38 2SD ($n = 6$), respectively.

[c]PIMMS (ThermoFinnigan Neptune) analysis. Average $^{143}Nd/^{144}Nd$ and $^{87}Sr/^{86}Sr$ ratios for J&M Nd standard and NBS 987 during the period of analysis were 0.511109 ± 12 2SD ($n = 12$) and 0.710254 ± 20 2SD ($n = 11$), respectively.

[d]Data from Skinner *et al.* (1994). Internal errors are reported as being 0.005% RSD. No reproducibility quoted for Sr or Nd standards. Nd ratios for samples have been re-normalized to a La Jolla value of 0.511862, whereas Sr ratios are taken as reported by Skinner *et al.* (1994).

All parent–daughter element concentrations used in the calculation of initial isotope ratios were obtained on the ELAN 6000 quadrupole ICP-MS at Durham University. ε_{Hf} values are calculated using the kimberlite ages in Table 1, a $^{176}Hf/^{177}Hf$ ratio for chondritic uniform reservoir (CHUR) of 0.282769 (Blichert-Toft & Albarede, 1997; normalized to a JMC475 value of 0.282160) and a Lu decay constant of 1.865×10^{-11}/a (Scherer *et al.*, 2001). Delta ε_{Hf} ($\Delta\varepsilon_{Hf}$) is the difference between the measured ε_{Hf} value and the oceanic basalt Nd–Hf regression of Vervoort *et al.* (1999) which is defined as $\varepsilon_{Hf(OIB)} = 1.33\ \varepsilon_{Nd} + 3.19$.

Table 2: Hf–Nd–Sr isotope data for megacryst phases from Group I kimberlites, and from the Phoenix blow Group II kimberlite, South Africa

Locality/mineral phase	Sample number	Lu	Hf	$^{176}Lu/^{177}Hf$	$^{176}Hf^{177}Hf_m$	ε_{Hfi}	$\Delta\varepsilon_{Hf}$	Sm	Nd	$^{147}Sm/^{144}Nd$	$^{143}Nd/^{144}Nd_m$	ε_{Ndi}	Rb	Sr	$^{87}Sr/^{86}Sr_m$
Premier (1180 Ma)															
Gt	PREM GT-1	0.624	2.4	0.036994	0.282978 (10)[3]	4.6	−2.6	1.29	1.59	0.515	0.515084 (12)	3	—	—	—
Cpx	PREM CPX-1	0.018	0.5305	0.004837	0.282225 (80)[3]	3.3	−6.3	1.572	5.98	0.1595	0.512595 (10)	4.8	—	—	—
Il	PREM IL-1	0.1	11.85	0.000121	0.282096 (24)[1]	2.4	−3.5	0.016	0.1	0.0963	0.511966 (15)	2.1	0.2	3.9	0.708345 (8)
Frank Smith (114 Ma)															
Gt	PHN 3240−1	0.49	2.25	0.031044	0.282751 (13)[2]	−0.44	−8.3	1.06	1.33	0.4805	0.513031 (18)	3.5	—	—	—
Gt	PHN 3240−2	0.5	2.07	0.034432	0.282785 (12)[2]	0.5	−6.8	1.21	1.52	0.4803	0.513008 (10)	3.1	—	—	—
Gt	PHN 3240−3	0.59	2.91	0.028902	0.282761 (12)[2]	0.07	−6.1	0.91	1.01	0.5426	0.513012 (48)	2.2	—	—	—
IL	PHN 3241−1	0.004	20.5	0.000028	0.282615 (54)[1]	−2.9	−1	0.02	0.08	0.1517	0.512407	−3.9	0.23	9.96	0.705112 (12)
IL	PHN 3241−1rpt	0.004	20.5	0.000028	0.282597 (8)[1]	−3.6	−1.6								
IL	PHN 3241−2	0.005	23.99	0.000029	0.282636 (18)[1]	−2.2	−7.6	0.02	0.14	0.1011	0.512652	1.7	0.28	0.67	0.705657 (16)
Monastery (90 Ma)															
Gt	ROM-263 GT-25	0.74	2.86	0.03689	0.282799 (7)[3]	0.85	−6.4	1.65	1.99	0.5021	0.512974 (10)	3	0.1	0.5	0.703552 (8)
Gt	ROM-263 GT-36	1.3	6.22	0.029754	0.282766 (5)[3]	0.11	−7.1	1.83	1.74	0.6382	0.513052 (10)	3			
Gt	ROM-263 GT-44	0.72	3.04	0.033948	0.282775 (9)[3]	0.18	−7	1.7	2.38	0.4326	0.512932 (12)	3	0.1	0.7	0.704132 (10)
Ilm	MON IL-1	0.01	15.11	0.000094	0.282734 (12)[1]	0.74	−7.6	0.05	0.198	0.1532	0.512812 (19)	3.9	0.273	1.64	0.704728 (14)
Ilm	ROM-264 IL-08	0.018	24.46	0.000047	0.282707 (6)[3]	−0.21	—	—	—		—	—	—	—	—
Ilm	ROM-264 IL-08rpt	0.018	24.46	0.000047	0.282736 (6)[3]	0.81	—	—	—		—	—	—	—	—
Ilm	ROM-264 IL-13	0.01	15.95	0.000072	0.282703 (6)[3]	−0.35	—	—	—		—	—	—	—	—
Ilm	ROM-264 IL-13rpt	0.01	15.95	0.000072	0.282749 (11)[3]	1.3	—	—	—		—	—	—	—	—
Ilm	ROM-264 IL-42	0.01	34.04	0.000034	0.282733 (5)[3]	0.71	−5.6	0.4	2.67	0.0904	0.512695 (10)	2.3	—	—	—
Ilm	ROM-264 IL-42rpt	0.01	34.04	0.000034	0.282743 (5)[3]	1.1	−5.2								
Phlog	GMN-98 PHLOG-1	0.01	0.26	0.000548	0.282731 (26)[3]	0.62	—	—	—		—	—	—	—	—
Cpx/**Ilm**	ROM-271 IL-10	0.01	25.62	0.000028	0.282734 (3)[3]	0.75		—	—		—	—	—	—	—
Cpx/Il	ROM-271 IL-10	0.033	6.99	0.000673	0.282735 (18)[3]	0.75	−6	3.33	12.51	0.1618	0.512754 (8)	2.7	—	—	—
Cpx/**Ilm**	MON-25 cpx-il	0.01	19.861	0.000043	0.282721 (3)[3]	0.28		—	—	—	—	—	—	—	—
Zir/ilm	ROM-121 Z098 (pit1)	—	—	0.000015	0.282735 (8)[4]	0.78	—	—	—	—	—	—	—		—
Zir/**Ilm**	ROM-121 Z098	0.01	23.94	0.000024	0.282729 (3)[3]	0.57	−5.3	0.15	0.94	0.0965	0.512682 (8)	2	0.2	2.5	0.703804 (8)

Table 2: Continued

Locality/mineral phase	Sample number	Lu	Hf	$^{176}Lu/^{177}Hf$	$^{176}Hf^{177}Hf_m$	ε_{Hfi}	$\Delta\varepsilon_{Hf}$	Sm	Nd	$^{147}Sm/^{144}Nd$	$^{143}Nd/^{144}Nd_m$	ε_{Ndi}	Rb	Sr	$^{87}Sr/^{86}Sr_m$
Zir/Ilm	ROM-121 Z005 (pit 1)	—	—	0.000014	0.282728 (8)[4]	0.53	—	—	—	—	—	—	—	—	—
Zir/**Ilm**	ROM-121 Z005	0.01	43.29	0.000017	0.282738 (4)[3]	0.89	—	—	—	—	—	—	—	—	—
Zir/**Ilm**	ROM-121 Z005 rpt	0.01	43.29	0.000017	0.282730 (4)[3]	0.6	—	—	—	—	—	—	—	—	—
Zir/Ilm	ROM-121 Z026 (pit 1)	—	—	0.000005	0.282714 (8)[4]	0.05	—	—	—	—	—	—	—	—	—
Zir/Ilm	ROM-121 Z026 (pit 2)	—	—	0.000005	0.282719 (7)[4]	0.22	—	—	—	—	—	—	—	—	—
Zir/Ilm	ROM-121 Z026 (pit 3)	—	—	0.000049	0.282731 (8)[4]	0.64	—	—	—	—	—	—	—	—	—
Zir/Ilm	ROM-121 Z026 (pit 4)	—	—	0.000038	0.282717 (9)[4]	0.14	—	—	—	—	—	—	—	—	—
Zir/**Ilm**	ROM-121 Z026	0.01	28.43	0.00002	0.282737 (5)[3]	0.85	—	—	—	—	—	—	—	—	—
Zir/Ilm	ROM-121 Z052 (pit 1)	—	—	0.000004	0.282708 (7)[4]	−0.17	—	—	—	—	—	—	—	—	—
Zir/Ilm	ROM-121 Z052 (pit 2)	—	—	0.000005	0.282726 (8)[4]	0.46	—	—	—	—	—	—	—	—	—
Zir/**Ilm**	ROM-121 Z052	0.01	41.88	0.000014	0.282736 (5)[3]	0.82	—	—	—	—	—	—	—	—	—
Jagersfontein (86 Ma)															
Gt	JAG-GT1	0.6	2.02	0.04234	0.282821 (11)[3]	1.33	−6.9	1.06	1.27	0.5064	0.513008 (10)	3.8	—	—	—
Gt	JAG-GT2	0.56	2.03	0.03932	0.282697 (8)[3]	−2.88	−9	1.19	1.61	0.4485	0.512893 (22)	2.2	—	—	—
Cpx	FRB 990	0.02	2.86	0.00095	0.282751 (46)[3]	1.21	−3	3.8	17.68	0.1303	0.512567 (6)	0.8	—	—	—
Orapa (92 Ma)															
Gt	OR-GT1	0.51	1.92	0.03786	0.282901 (10)[3]	4.4	−6.2	1.11	1.28	0.5262	0.513120 (20)	5.5	—	—	—
Gt	OR-GT2	0.57	2.22	0.0366	0.282878 (8)[3]	3.66	−4.8	1.2	1.34	0.543	0.512757 (12)	4	—	—	—
Thaba Putsoa (90 Ma)															
Gt	TP-GT1	0.57	2.14	0.03797	0.282848 (12)[3]	2.5	−7	1.22	1.47	0.5036	0.513062 (10)	4.7	—	—	—
Gt	TP-GT2	0.71	3.31	0.03058	0.282726 (7)[3]	−1.4	−8.4	1.72	2	0.5214	0.512977 (10)	2.9	—	—	—
Ilm	TP-ILM1	0.004	39.21	0.000015	0.282746 (5)[3]	1.2	—	—	—	—	—	—	—	—	—
Ilm	TP-ILM1	0.005	35.52	0.00002	0.282737 (5)[3]	0.85	—	—	—	—	—	—	—	—	—
Ilm	TP-ILM3	0.004	27.84	0.000021	0.282734 (5)[3]	0.75	—	—	—	—	—	—	—	—	—
Cpx	TP-CPX1	0.031	0.42	0.0105	0.282884 (47)[3]	5.4	−1.6	1.65	5.94	0.1683	0.512770 (6)	2.9	—	—	—
Cpx	TP-CPX2	0.033	1	0.0047	0.282919 (57)[3]	7	−2.4	1.7	6.04	0.1704	0.512862 (10)	4.7	—	—	—
Cpx	TP-CPX3	0.03	0.392	0.0109	0.282894 (169)[3]	5.8	−1.4	1.56	5.77	0.1643	0.512771 (8)	3	—	—	—
Phlog	TP-PHLOG1	0.001	0.268	0.00053	0.282748 (24)[3]	1.2	—	—	—	—	—	—	—	—	—

Locality/mineral phase	Sample number	Lu	Hf	$^{176}Lu/^{177}Hf$	$^{176}Hf^{177}Hf_m$	ε_{Hfi}	$\Delta\varepsilon_{Hf}$	Sm	Nd	$^{147}Sm/^{144}Nd$	$^{143}Nd/^{144}Nd_m$	ε_{Ndi}	Rb	Sr	$^{87}Sr/^{86}Sr_m$
Kao (90 Ma)															
Gt	KAO-GT1	—	—	—	—	—	—	1.48	1.89	0.4757	0.512976 (12)	3.4	—	—	—
Gt	KAO-GT2	0.5	2.07	0.03443	0.282859 (12)[3]	3.1	−5.7	0.92	0.87	0.646	0.513119 (16)	4.2	—	—	—
Ilm	KAO-ILM1	0.004	24.94	0.000023	0.282673 (6)[3]	−1.4	—	—	—	—	—	—	—	—	—
Ilm	KAO-ILM3	0.004	13.95	0.000061	0.282683 (5)[3]	−1.1	—	—	—	—	—	—	—	—	—
Phoenix Blow, Star Mine (135 Ma)															
Gt	SJH-90 GT-01	0.583	0.583	0.052783	0.282546 (8)[3]	−9.5	−1.9	1.4	2.02	0.4228	0.512410 (14)	−8.1	0.2	1	0.707733 (8)
Gt	SJH-90 GT-013	0.6	0.601	0.042027	0.282646 (9)[3]	−5.1	3.6	1.52	1.94	0.4753	0.512415 (14)	−8.9	0.3	1.9	0.707945 (8)

All sample data are normalized to the same accepted standard values given in the legend to Table 1.

Hf isotope compositions of the megacrysts were determined by a combination of conventional TIMS, solution-mode PIMMS and laser ablation-mode PIMMS. Lu and Yb corrections on ^{176}Hf were made using the methodology of Nowell & Parrish (2001) and Nowell *et al.* (2003). Method of analysis for individual samples is indicated by the superscript symbols in the $^{176}Hf/^{177}Hf_m$ column.

[1]TIMS analysis (MAT 262). Average $^{176}Hf/^{177}Hf$ ratio and external reproducibility for JMC 475 was 0.282169 ± 14 2SD ($n = 24$).

[2]Solution-mode PIMMS analysis (Plasma54). Average $^{176}Hf/^{177}Hf$ ratio and external reproducibility for JMC 475 was 0.282172 ± 19 2SD ($n = 99$).

[3]Solution-mode PIMMS analysis (Plasma54). Average $^{176}Hf/^{177}Hf$ ratio and external reproducibility for JMC 475 was 0.282159 ± 12 2SD ($n = 24$).

[4]Laser ablation mode PIMMS analysis (Plasma54). Average $^{176}Hf/^{177}Hf$ ratio and external reproducibility for JMC 475 was 0.282155 ± 21 2SD ($n = 12$). The average $^{176}Hf/^{177}Hf$ ratio and reproducibility for the zircon ablation standard 91500 (Weidenbeck *et al.*, 1995) after re-normalization to a JMC 475 value of 0.28216 was 0.282279 ± 27 2SD ($n = 4$ pits). This is well within error of the TIMS value of Weidenbeck *et al.* (1995), 0.282302 ± 8 2SD ($n = 7$), corrected to a JMC 475 value of 0.28216.

Sr compositions on garnet and ilmenite phases were determined by conventional TIMS at NIGL during which the average $^{87}Sr/^{86}Sr$ ratio for NBS 987 was 0.710189 ± 23 ($n = 21$). Nd isotopic compositions of garnet, ilmenite (except PHN3241-1, PHN3241-1 and MON-1) and cpx phases were determined by TIMS at NIGL, during which time the average $^{143}Nd/^{144}Nd$ for the La Jolla Nd std was 0.511894 ± 21 ($n = 34$). Ilmenites PHN3241-1, PHN3241-1 and MON-1 were analysed for Nd isotope compositions at The Deptartment of Terrestrial Magmatism using the NdO^+ TIMS method. The average $^{143}Nd/^{144}Nd$ for La Jolla during analysis of the ilmenites was 0.511832 ± 25 2SD.

Initial Sr and Nd isotope ratios for garnet, ilmenite and cpx megacryst phases are calculated using the host kimberlite eruption age and constants given in Table 1. This also applies to initial Hf isotope ratios for garnet and cpx phases. The measured Hf isotope ratios of ilmenites and zircons are age invariant, due to the extremely low Lu/Hf ratio, and are therefore also taken as the initial ratios. εHf values are calculated using a $^{176}Hf/^{177}Hf$ ratio for CHUR of 0.282769 (Blichert-Toft and Albarede, 1997; re-normalised to a JMC 475 value of 0.28216).

Table 3: Hf isotopic compositions for discrete mono-mineralic zircons from various Group I SA kimberlites

Locality	$^{176}Lu/^{177}Hf$ NIGL	$^{176}Hf/^{177}Hf_n$	ε_{Hfl}	$^{176}Lu/^{177}Hf$ DTM	$^{176}Hf/^{177}Hf_n$	ε_{Hfl}	$^{176}Lu/^{177}Hf$ AHIGL	$^{176}Hf/^{177}Hf_n$	ε_{Hfl}
Monastery									
BZ 6 1-B	0·0000060	0·282724 (6)[1]	0·39						
BZ 8 7-B	0·0000070	0·282735 (6)[1]	0·78						
BZ 9 N.R.	0·0000110	0·282728 (6)[1]	0·53						
BZ 10 10—1B	0·0000010	0·282713 (6)[1]	0						
BZ 11 10—2B	0·0000010	0·282716 (6)[1]	0·11						
BZ 13 3-C	0·0000050	0·282737 (6)[1]	0·85						
BZ 14 8-C	0·0000110	0·282723 (6)[1]	0·36						
BZ 15 5-C	0·0000100	0·282730 (6)[1]	0·6						
BZ 16 N.A.	0·0000200	0·282718 (6)[1]	0·18						
BZ 17 10—3C	0·0000220	0·282723 (6)[1]	0·36						
Orapa									
PHN 1613 A 1	0·0000235	0·282766 (8)[2]	1·92	0·0000407	0·282769 (11)	2·03	0·0000355	0·282776 (12)[3]	2·28
PHN 1613 A 2	0·0000310	0·282745 (10)[2]	1·18				0·0000429	0·282769 (12)[3]	2·03
PHN 1613 B 1	0·0000162	0·282752 (11)[2]	1·43	0·0000164	0·282774 (10)	2·2	0·0000220	0·282758 (10)[3]	1·64
PHN 1613 B 2	0·0000169	0·282755 (8)[2]	1·53				0·0000233	0·282763 (12)[3]	1·82
PHN 1613 C 1	0·0000194	0·282745 (14)[2]	1·18	0·0000221	0·282747 (13)	1·25	0·0000295	0·282751 (14)[3]	1·39
PHN 1613 C 2	0·0000163	0·282738 (12)[2]	0·93				0·0000221	0·282744 (12)[3]	1·14
PHN 1613 D 1	0·0000213	0·282750 (6)[2]	1·35	0·0000237	0·282769 (13)	2·03	0·0000291	0·282768 (6)[3]	1·99
PHN 1613 D 2	0·0000212	0·282778 (8)[2]	2·34				0·0000273	0·282769 (4)[3]	2·03
PHN 1613 E 1	0·0000065	0·282366 (10)[2]	−12·2	0·0000074	0·282372 (11)	−12	0·0000091	0·282371 (5)[3]	−12
PHN 1613 E 2	0·0000063	0·282361 (7)[2]	−12·4				0·0000095	0·282369 (5)[3]	−12·1
PHN 1613 F 1	0·0000269	0·282724 (10)[2]	0·43	0·0000400	0·282749 (12)	1·31	0·0000319	0·282756 (5)[3]	1·57
PHN 1613 F 2	0·0000360	0·282760 (7)[2]	1·71				0·0000376	0·282772 (4)[3]	2·13
PHN 1613 G 1	0·0000153	0·282757 (12)[2]	1·6	0·0000216	0·282780 (13)	2·43	0·0000205	0·282759 (6)[3]	1·68
PHN 1613 G 2	0·0000187	0·282763 (12)[2]	1·81				0·0000229	0·282765 (5)[3]	1·89
PHN 1613 H 1	0·0000183	0·282754 (19)[2]	1·5	0·0000160	0·282759 (9)	1·68	0·0000249	0·282758 (6)[3]	1·64
PHN 1613 H 2	0·0000182	0·282763 (14)[2]	1·81				0·0000297	0·282764 (6)[3]	1·85
PHN 1613 I 1	0·0000211	0·282755 (11)[2]	1·53	0·0000269	0·282767 (11)	1·95	0·0000308	0·282754 (5)[3]	1·5
PHN 1613 I 2	0·0000247	0·282744 (13)[2]	1·14				0·0000293	0·282754 (5)[3]	1·5
PHN 1613 J 1	0·0000078	0·282343 (11)[2]	−13	0·0000136	0·282368 (11)	−12·1	0·0000107	0·282365 (5)[3]	−12·3
PHN 1613 J 2	0·0000137	0·282359 (10)[2]	−12·5				0·0000176	0·282367 (6)[3]	−12·2
PHN 1613 K 1	0·0000073	0·282303 (14)[2]	−14·5	0·0000085	0·282322 (10)	−13·8	0·0000098	0·282316 (7)[3]	−14
PHN 1613 K 2	0·0000110	0·282305 (15)[2]	−14·4				0·0000148	0·282314 (5)[3]	−14·1
PHN 1613 L 1	0·0000081	0·282314 (14)[2]	−14·1	0·0000101	0·282323 (9)	−13·8	0·0000068	0·282316 (5)[3]	−14
PHN 1613 L 2	0·0000062	0·282293 (15)[2]	−14·8				0·0000103	0·282315 (6)[3]	−14
PHN 1613 M 1	0·0000086	0·282339 (11)[2]	−13·2	0·0000093	0·282363 (11)	−12·3	0·0000055	0·282363 (6)[3]	−12·3
PHN 1613 M 2	0·0000104	0·282354 (16)[2]	−12·7				0·0000158	0·282362 (5)[3]	−12·4
PHN 1613 N 1	0·0000082	0·282726 (13)[2]	0·51	0·0000082	0·282770 (9)	2·08	0·0000103	0·282757 (5)[3]	1·6
PHN 1613 N 2	0·0000051	0·282723 (10)[2]	0·4				0·0000047	0·282756 (5)[3]	1·57
PHN 1613 O 1	0·0000233	0·282762 (14)[2]	1·78	0·0000209	0·282761 (11)	1·76	0·0000359	0·282761 (6)[3]	1·75
PHN 1613 O 2	0·0000167	0·282732 (11)[2]	0·72				0·0000186	0·282757 (5)[3]	1·6
Kaalvallie									
ZirA-1	0·0000037	0·282738 (17)[2]	0·79				0·0000054	0·282740 (8)[4]	0·85
ZirA-2	0·0000036	0·282717 (17)[2]	0·04				0·0000059	0·282746 (4)[4]	1·06
ZirA-3	0·0000035	0·282718 (18)[2]	0·08						
ZirA-4	0·0000033	0·282734 (15)[2]	0·65						
ZirB-1	0·0000081	0·282748 (22)[2]	1·14						
ZirB-2	0·0000077	0·282772 (24)[2]	1·99						
ZirB-3	0·0000069	0·282770 (20)[2]	1·92						
ZirB-4	0·0000066	0·282728 (21)[2]	0·43						
ZirC-1	0·0000057	0·282757 (27)[2]	1·46				0·0000088	0·282782 (4)[4]	2·33
ZirC-2	0·0000060	0·282772 (25)[2]	1·99				0·0000087	0·282780 (4)[4]	2·26
ZirD-1	0·0000102	0·282737 (24)[2]	0·75						
ZirD-2	0·0000107	0·282717 (25)[2]	0·04						
ZirE-1							0·0000158	0·282758 (4)[4]	1·49
ZirE-2							0·0000156	0·282745 (4)[4]	1·03

Table 3: continued

Locality	$^{176}Lu/^{177}Hf$ NIGL	$^{176}Hf/^{177}Hf_n$	ε_{Hfi}	$^{176}Lu/^{177}Hf$ DTM	$^{176}Hf/^{177}Hf_n$	ε_{Hfi}	$^{176}Lu/^{177}Hf$ AHIGL	$^{176}Hf/^{177}Hf_n$	ε_{Hfi}
ZirF-1							0·0000180	0·282763 (3)[4]	1·66
ZirF-2							0·0000169	0·282752 (4)[4]	1·27
ZirG-1							0·0000128	0·282751 (4)[4]	1·24
ZirG-2							0·0000132	0·282754 (5)[4]	1·34
ZirH-1							0·0000175	0·282774 (5)[4]	2·05
ZirH-2							0·0000166	0·282774 (6)[4]	2·05
ZirI-1							0·0000156	0·282773 (4)[4]	2·02
ZirI-2							0·0000154	0·282763 (3)[4]	1·66
ZirJ-1							0·0000056	0·282748 (4)[4]	1·14
ZirJ-1							0·0000061	0·282747 (4)[4]	1·1
Gansfontein									
PMD-99−019ZrP1							0·0000089	0·282701 (6)[4]	−0·2
PMD-99−019ZrP2							0·0000096	0·282710 (4)[4]	0·12
PMD-99−003ZrP1							0·0000188	0·282727 (7)[4]	0·72
PMD-99−003ZrP2							0·0000145	0·282712 (6)[4]	0·19
PMD-99−074ZrP1							0·0000151	0·282715 (5)[4]	0·3
PMD-99−074ZrP2							0·0000095	0·282705 (4)[4]	−0·06
PMD-99−017ZrP1							0·0000077	0·282704 (8)[4]	−0·09
PMD-99−017ZrP2							0·0000103	0·282702 (10)[4]	−0·16
Kampfersdam									
FRB 248c	0·0000221	0·282721 (10)[2]	0·22						
Mothae pipe									
PHN 1931−1	0·0000077	0·282711 (7)[2]	−0·06						
PHN 1931−2	0·0000149	0·282718 (7)[2]	0·19						
PHN 1931−3	0·0000073	0·282723 (7)[2]	0·37						
PHN 1931−4	0·0000190	0·282718 (7)[2]	0·19						

Hf isotope compositions were determined by a combination of solution mode PIMMS and laser ablation-mode PIMMS at three different laboratories, as indicated. Lu and Yb corrections on ^{176}Hf were made using the methodology of Nowell & Parrish (2001) and Nowell *et al*. (2003). All sample data are normalized to the accepted JMC475 standard composition given in the caption to Table 1. Where appropriate, the method of analysis for individual samples is indicated by the superscript symbols in the $^{176}Hf/^{177}Hf_m$ column.

NIGL data:

[1]Solution-mode PIMMS analysis (P54). Average $^{176}Hf/^{177}Hf$ ratio and external reproducibility for JMC 475 was 0.282172 ± 19 2SD ($n = 99$).

[2]Laser ablation mode PIMMS analysis (Axiom). Average $^{176}Hf/^{177}Hf$ ratio and external reproducibility for both pure and Yb+Lu-doped JMC 475 was 0.282175 ± 20 2SD ($n = 19$). The average $^{176}Hf/^{177}Hf$ ratio and reproducibility for the zircon ablation standard 91500 (Weidenbeck *et al*., 1995) after re-normalization to a JMC 475 value of 0.28216 was 0.282286 ± 73 2SD ($n = 15$ pits). This is well within error of the TIMS value of Weidenbeck *et al*. (1995), 0.282302 ± 8 2SD ($n = 7$), normalized to a JMC 475 value of 0.28216. Despite the Yb−Lu correction on ^{176}Hf for 91500 being about 10 times smaller than that for the Yb−Lu doped JMC 475 standards, the reproducibility of $^{176}Hf/^{177}Hf$ for 91500 (259 ppm) is greater than three times worse than for the JMC 475 solution standards (71 p.p.m.), which suggests that 91500 is somewhat heterogeneous in terms of Hf isotopic composition.

DTM data:

Laser ablation mode PIMMS analysis (Axiom). Average $^{176}Hf/^{177}Hf$ ratio and external reproducibility for pure JMC 475 standard only was 0.282141 ± 16 2SD ($n = 7$).

AHIGL data:

[3]Laser ablation mode PIMMS analysis (ThermoFinnigan Neptune). Average $^{176}Hf/^{177}Hf$ ratio and external reproducibility for both pure and Yb+Lu-doped JMC 475 was 0.282158 ± 4 2SD ($n = 17$).

[4]Laser ablation mode PIMMS analysis (ThermoFinnigan Neptune). Average $^{176}Hf/^{177}Hf$ ratio and external reproducibility for both pure and Yb+Lu-doped JMC 475 was 0.282155 ± 7 2SD ($n = 12$).

For the Orapa zircons, the NIGL and DTM Hf isotope data generally agree to better than 1ε unit (except for PHN1613N, which is slightly worse at 1.6 ε units), with the average difference being 0.56 ε units. For the NIGL and AHIGL data sets the agreement is slightly better with an average difference of only 0.38 ε units. Again, however, the difference for PHN1613N, and also PHN1613F, is slightly greater than 1ε unit. The agreement between the AHIGL and DTM data sets is extremely good, including samples PHN1613N, and PHN1613F, with an average difference of only 0.15 ε units. Indeed, five of the 14 samples reproduce to better than 0.04 ε units. On the basis of the close agreement between the AHIGL and DTM data-sets, we use the more extensive and higher precision AHIGL data set to define the range in Hf isotopic composition for the Orapa zircon suite.

The agreement between NIGL and AHIGL Hf isotope data for the two Kaalvallie zircons is better than 0.8 ε units although the reproducibility of the AHIGL Neptune data for the two repeat analyses of each zircon is considerably better (<10 ppm).

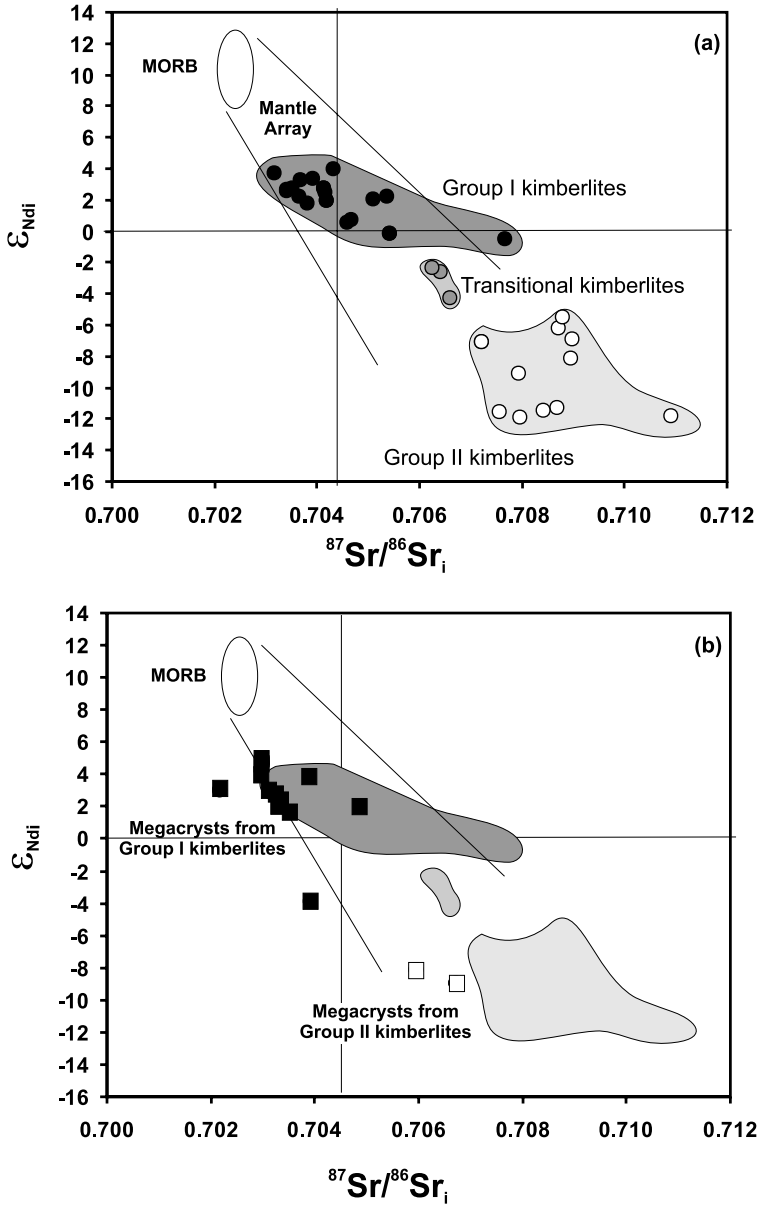

Fig. 2. (a) ε_{Ndi} versus $^{87}Sr/^{86}Sr_i$ for Group I (black circles), Transitional (grey circles) and Group II kimberlites (open circles), based on new data presented in Table 1. Field for mid-ocean ridge basalts (MORB) and the mantle array are shown schematically. (b) ε_{Ndi} versus $^{87}Sr/^{86}Sr_i$ for megacrysts from Group I kimberlites (black squares) and Group II kimberlites (open squares), together with the fields for kimberlites (field for Group II kimberlites excludes the Swartruggens samples).

et al. (1995) are distinct from Group I megacrysts in that they have less radiogenic Nd and more radiogenic Sr. In common with the relationships shown between Group I megacrysts and their hosts, the Nd isotopic compositions of Group II megacrysts overlap those of their hosts, whereas their Sr isotope compositions are less radiogenic. In contrast to Sr isotope systematics, both Group I and Group II megacrysts show very similar Nd–Hf isotope systematics to their host kimberlites (Fig. 3a and b). With a few exceptions, the megacrysts from Group I kimberlites plot within the Nd–Hf isotope field of their hosts. Although the absolute ranges in Nd and Hf isotope compositions for the megacrysts and kimberlites are slightly different, the seven megacryst suites from Group I kimberlites all plot below the mantle array, with negative $\Delta\varepsilon_{Hf}$ values ranging from −1 to −9 (Fig. 4b). This range is almost exactly analogous to the range for the kimberlites (Fig. 5). Hence, Group I kimberlites and the parental megacryst magma both share the characteristic of having negative $\Delta\varepsilon_{Hf}$ signatures.

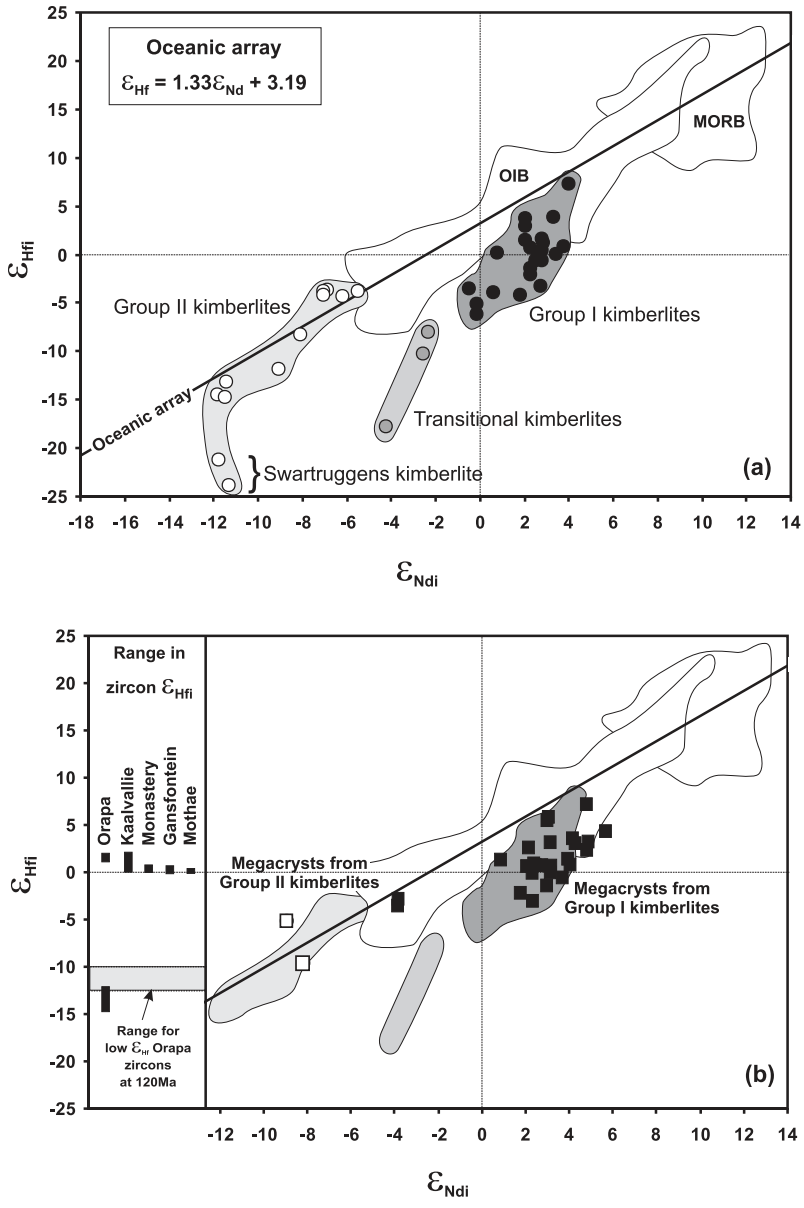

Fig. 3. (a) ε_{Hfi}–ε_{Ndi} for Group I, Group II and Transitional kimberlites from Southern Africa (symbols as in Fig. 2a), together with fields for oceanic basalts. Data source for MORB and OIB can be found in the captions to Fig. 1 and Appendix 1 of Nowell *et al.* (1998). (b) ε_{Hfi}–ε_{Ndi} for Cr-poor megacrysts from Group I kimberlites and Group II kimberlites (symbols as in Fig. 2b), together with fields for whole-rock kimberlites (field for Group II kimberlites excludes the Swartruggens samples). Also shown on the left-hand side are the ranges in ε_{Hfi} for zircon megacrysts from the Orapa, Kaalvallie, Monastery, Gansfontein and Mothae Group I kimberlites. The mantle array is taken from Vervoort *et al.* (1999) and defined as $\varepsilon_{Hf} = 1.33\ \varepsilon_{Nd} + 3.19$.

Low-Cr megacrysts from individual kimberlites have a relatively restricted isotopic range. For instance, despite the known complexity of elemental variations within the Monastery megacrysts, possibly resulting from multiple generations of growth (Gurney *et al.*, 1979, 1998; Moore *et al.*, 1992), this assemblage has a remarkably limited variation in Hf isotope composition. The entire range of ε_{Hfi} values (−0.35 to 1.1) for the megacryst suite is only 1.45 epsilon units, with no systematic variation between phases. This essentially constant ε_{Hfi} contrasts with the 2.4 epsilon units' variation shown by the two whole-rock kimberlite samples from Monastery (Table 1) and probably attests to the more complex interactions experienced by the kimberlites en route to the surface. Nd isotope compositions of the Monastery megacrysts are marginally more variable than for Hf (ε_{Ndi} from 2.0 to 3.9). Only the megacrysts from Frank Smith show significant Nd isotope variability, but this range is due to a single ilmenite that

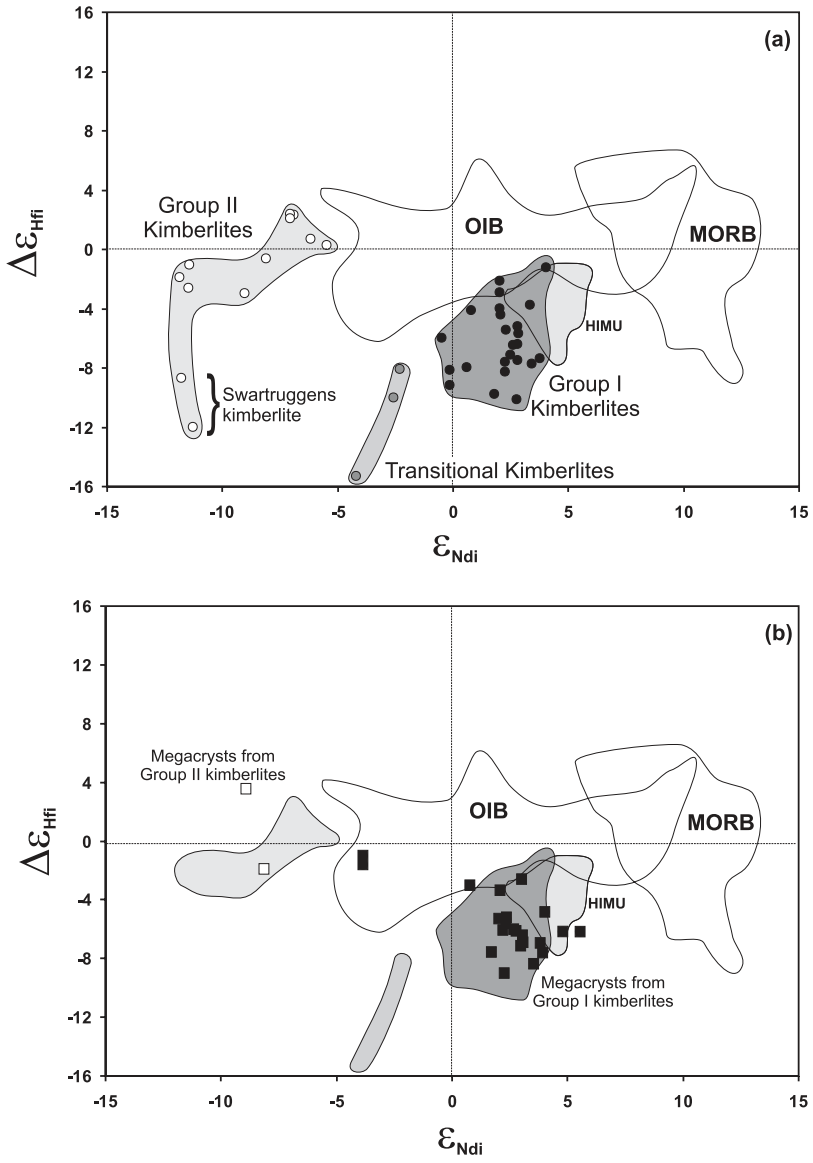

Fig. 4. (a) $\Delta\varepsilon_{Hfi}$–ε_{Ndi} for Group I, Group II and Transitional kimberlites from Southern Africa (symbols as in Fig. 2a), together with fields for oceanic basalts (data sources as in Fig. 3). (b) $\Delta\varepsilon_{Hfi}$–ε_{Ndi} for Cr-poor megacrysts from Group I and Group II kimberlites, together with fields for whole-rock kimberlites (field for Group II kimberlites excludes the Swartruggens samples). $\Delta\varepsilon_{Hf}$ is defined as $\varepsilon_{Hf} = (1.33\ \varepsilon_{Nd} + 3.19)$ such that a sample with positive $\Delta\varepsilon_{Hf}$ lies above and a sample with negative $\Delta\varepsilon_{Hf}$ lies below the mantle array of Vervoort *et al.* (1999).

has significantly lower ε_{Ndi}. We do not at present understand the cause of this variation but this individual ilmenite could be from a distinct generation of megacrysts, unrelated to the main suite that has isotopic compositions similar to their host kimberlite (see below).

Nd isotope compositions have not yet been determined for zircons or zircons from bi-mineralic intergrowths because of the low Nd concentrations. Nevertheless, the observed Hf isotope equilibrium between zircon and ilmenite from bi-mineralic intergrowths (Table 2) suggests that the zircon Nd isotope composition should also be in equilibrium with that of the ilmenites and, hence, unradiogenic compared with other phases. For most zircons, between two and four spot-analyses were made of each grain and the replicates are generally within 0.5 epsilon Hf units (Table 3). Mono-mineralic zircons from Monastery, Kaalvallie, Kampfersdam, Gansfontein and Mothae have a very restricted range in ε_{Hfi} (−0.2 to +2.3; Table 3). In contrast, zircons from Orapa show a large range in ε_{Hfi} (−14.1 to +2.3) that can be divided into two distinct populations, one with a range of ε_{Hfi} from −12 to −14 and one with a range from 1.1 to +2.3 (Table 3, AHIGL data). Griffin *et al.* (2000) also defined two populations of zircons at Orapa and Jwaneng, based

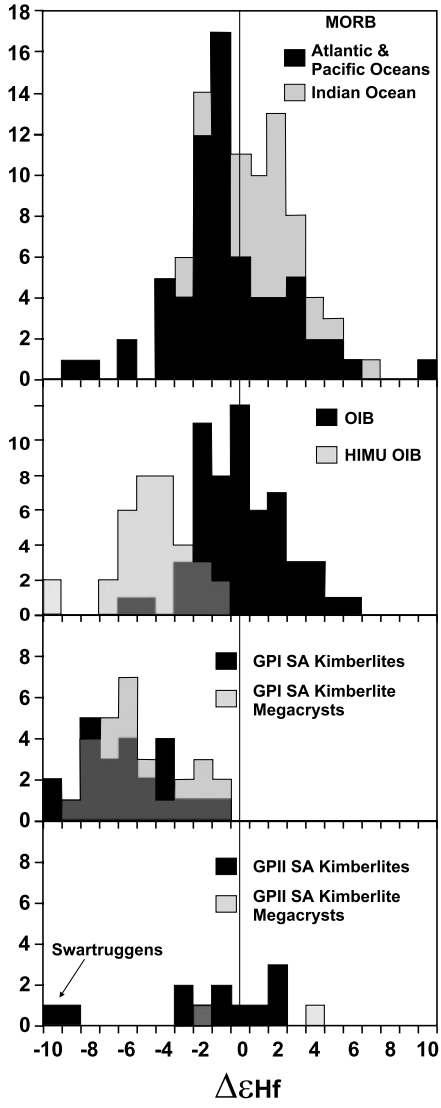

Fig. 5. Histogram of $\Delta\varepsilon_{Hf}$ in MORB, OIB, HIMU OIB, Southern African Group I and II kimberlites and their megacrysts. For Indian MORB, the data are added onto the Atlantic and Pacific data. For other combined histograms, the lighter shaded dataset is superimposed over the darker-shaded dataset, with the region of overlap shown by an intermediate level of shading. Data sources for MORB and OIB can be found in the captions to Fig. 1 and Appendix 1 of Nowell *et al.* (1998), together with additional data from Ballentine *et al.* (1997) and Chauvel & Blichert-Toft (2001). Although the dataset for OIB is not complete, additional data would not significantly alter the distribution about $\Delta\varepsilon_{Hf} = 0$.

on their Hf isotope compositions. Excepting these low ε_{Hf} zircons, the average Hf isotope composition of the bulk of the zircon megacrysts from Group I kimberlites is very tightly clustered and strikingly similar to the average composition of Group I megacryst suites as a whole (Fig. 3b).

Two low-Cr garnet megacrysts from the Group II Star kimberlite are isotopically distinct from the garnet megacrysts from the Group I kimberlites (Fig. 3b). The Star garnets plot very close to an extension of the mantle array (Fig. 4b; $\Delta\varepsilon_{Hf}$ −1.9 to 3.6) and are within the range of compositions determined for the Star kimberlite (N. Coe, unpublished data). Hence, for both Group I and Group II kimberlites, the low-Cr megacrysts generally have similar isotopic characteristics to their host kimberlites.

KIMBERLITE ISOTOPIC VARIATIONS: CRUSTAL CONTAMINATION OR MANTLE SIGNATURE?

It is generally believed that the high concentrations of Sr and Nd in kimberlites render their isotope signatures relatively immune to the effects of crustal contamination. Although this is true to a certain extent, the lower levels of Hf make it essential to carefully select samples for analysis that show minimal signs of crustal contamination and have trace element systematics, such as high Gd/Yb, that confirm this. All samples selected for this study were the freshest, least visibly contaminated hypabyssal facies samples available. They have the lowest contamination indices (C.I.: $(SiO_2 + Al_2O_3 + Na_2O)/(MgO + K_2O)$) of samples available from a given mine, high Gd/Yb, low SiO_2 and do not have positive Pb anomalies. The Group I samples have Yb contents <1 ppm. As such, we interpret the isotope systematics of our sample set as reflecting their mantle source compositions and/or processes operating in the mantle during kimberlite genesis and ascent.

Exceptions to the low levels of crustal contamination in our dataset may be the two samples from the Swartruggens dyke (14/6 and 15/1). The Swartruggens dykes are mineralogically different from all other Group II kimberlites in that they contain diverse Zr-silicates and quartz in many samples (Mitchell, 1995). Although no quartz has been reported in the Swartruggens samples analysed in this study [see Smith *et al.* (1985) for sample descriptions], these samples have higher C.I. than kimberlites from elsewhere (1.20 and 1.36) and they show a positive correlation between C.I. and $^{87}Sr/^{86}Sr$ that is suggestive of alteration or crustal contamination (Smith *et al.*, 1985). Because of the likelihood of a crustal influence on the isotopic signatures of these rocks, they are excluded from any further discussion of the nature of kimberlite source regions. We note that, for the kimberlites with low C.I. (close to unity), there is no correlation between C.I. and Hf–Nd–Sr isotope composition, indicating that crustal contamination is unlikely to explain the observed isotope variations.

An additional indication that the isotopic characteristics of the kimberlites are dominated by their mantle sources is the observed close matching of Nd–Hf isotope

compositions of the low-Cr megacryst suite with their host kimberlite and the overall consistency of the kimberlite and megacryst fields (Figs 4b and 5). Geothermometry studies place the crystallization of all kimberlite megacryst suites in the mantle (Nixon & Boyd, 1973). This, combined with the ability to hand-pick gem-quality mineral fragments from the megacrysts, excludes the influence of crustal components from their geochemistry. Megacrysts from Group I kimberlites have almost exactly the same range of displacements below the mantle array as the kimberlites (Fig. 5; Table 4.). This is a very strong indication that (a) the negative $\Delta\varepsilon_{Hf}$ signature is of mantle and not crustal origin and (b) the megacryst parental magmas were derived from a similar source, or combination of sources, to the kimberlites.

Table 4: Summary statistics for $\Delta\varepsilon_{Hf}$ in Group I kimberlites and their megacrysts

	SA GpI kimberlites $n = 24$	SA GpI kimberlite megacrysts $n = 28$
Mean	−6.2	−5.4
Standard error	0.48	0.44
Median	−6.4	−6.1
Mode	—	−1.6
Standard deviation	2.37	2.33
Sample variance	5.59	5.43
Kurtosis	−0.52	−0.83
Skewness	0.35	0.55
Range	8.9	8
Minimum	−10.1	−9
Maximum	−1.2	−1
Sum	−148	−150.4

Cr-POOR MEGACRYSTS–KIMBERLITE RELATIONSHIPS AND MEGACRYST ISOCHRON SYSTEMATICS

The precise relationship between the low-Cr megacryst suite and the host kimberlites is as yet unresolved (e.g. Nixon & Boyd, 1973; Harte & Gurney, 1981; Jones, 1987; Hops *et al.*, 1992; Smith *et al.*, 1995; Davies *et al.*, 2001; Moore & Lock, 2001). Some studies have reported small isotopic differences between the megacrysts and kimberlites. For instance, Davies *et al.* (2001) opted for a 'non-cognate' origin for megacrysts from Namibian kimberlites on the basis of differences in Sr–Nd–Pb isotope systematics. However, that study did not analyse megacrysts together with the host intrusion. Furthermore, the Pb isotopic compositions of kimberlites are very susceptible to crustal contamination and so it would be surprising if identical compositions were preserved in megacrysts formed towards the base of the lithosphere and kimberlites that have traversed and interacted with the crust prior to their crystallization. Differences between the megacrysts and their host kimberlites in this study are most apparent in their Sr isotope compositions. The less radiogenic Sr of the megacrysts may be a function of the incorporation of radiogenic Sr by kimberlites during their ascent through CLM and crust and/or subsequent alteration processes. We note that the least radiogenic Group I kimberlite Sr isotope compositions overlap the main megacryst field (Fig. 2b). At most localities, the Nd and Hf isotope variation between megacrysts is minor and their initial ratios are within error of those of the host kimberlite, especially when multiple analyses of the kimberlite are made. This isotopic similarity between megacrysts and their host kimberlite (Smith *et al.*, 1995; Fig. 3b) strongly supports some type of genetic relationship.

If the low-Cr megacryst suite has a genetic relationship to kimberlite, then we may expect its age to be either similar to the host kimberlite, or equivalent to a previous kimberlite event. In addition, where the age of the megacryst suite is similar to the host kimberlite, we would also expect their initial isotopic ratios to overlap. As noted above, comparisons of megacryst geochemistry with the host magmas require minimally contaminated whole-rock samples. A further complication is that megacrysts may crystallize from multiple batches of isotopically heterogeneous magma, at distinct time intervals. A clear indication of this complexity is seen in the range of ε_{Hf} values for zircon megacrysts from Orapa (Table 3; Fig. 3b). If the process of megacryst formation involves interaction/assimilation with their surrounding CLM, it is important to examine the *entire* crystallizing assemblage, especially the early crystallizing phases, to properly understand the significance of these processes and to be able to constrain the parental magma composition. Early isotopic studies on megacrysts focused on the Rb–Sr and Sm–Nd isotope systems, which precluded examination of late crystallizing phases, such as ilmenite and zircon, because of very low daughter element concentrations (Kramers *et al.*, 1981; Jones, 1987; Hops *et al.*, 1992). An advantage of the Lu–Hf isotope system is that all phases contain sufficient Hf for high-precision isotopic analysis. Furthermore, late crystallizing phases such as ilmenite and zircon have particularly high Hf contents (tens of ppm to 1.5 wt %, respectively) coupled with very low Lu/Hf ratios, so that $^{176}Hf/^{177}Hf$ ratios are essentially time-invariant and allow estimation of accurate initial ratios.

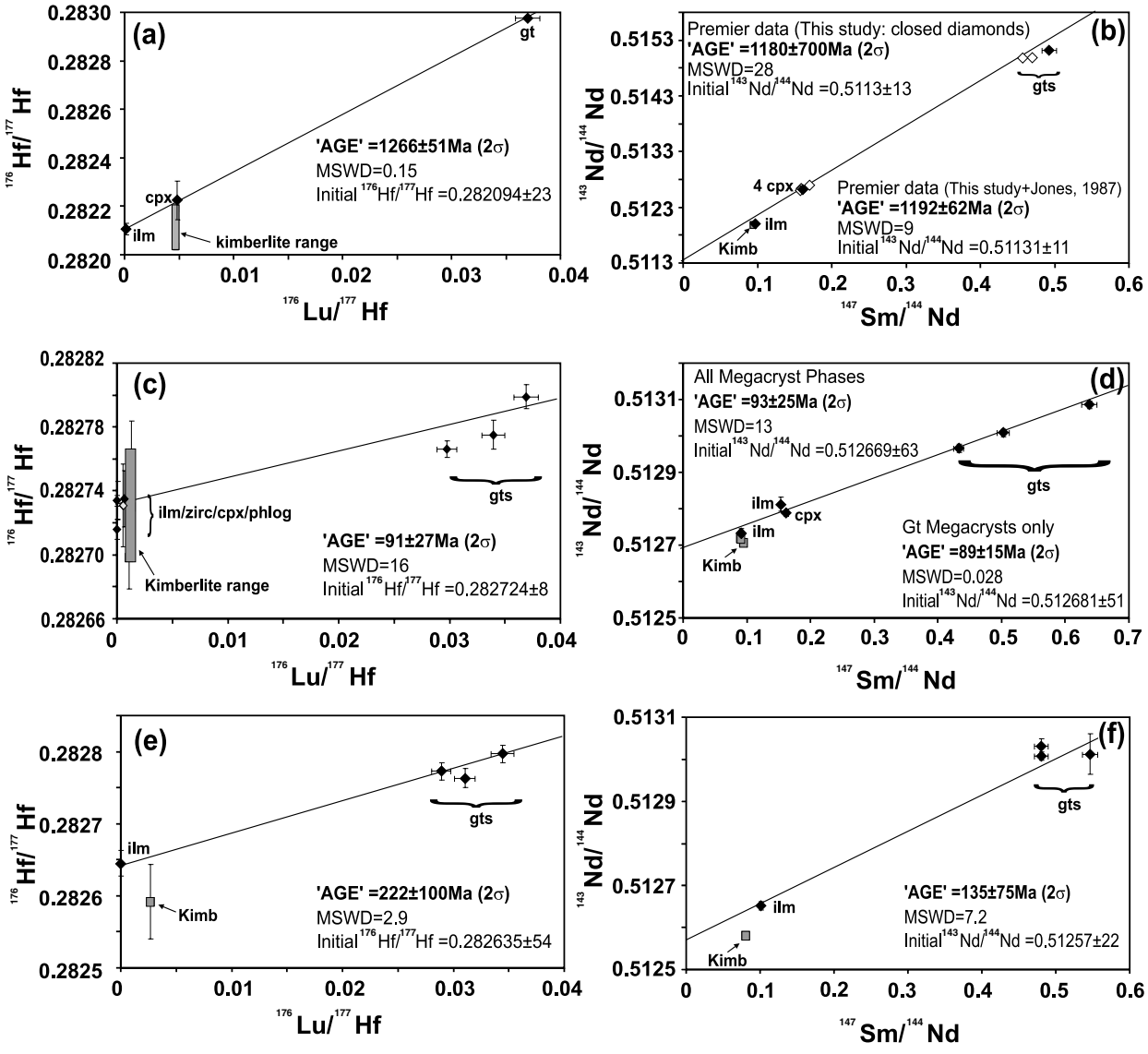

Fig. 6. Lu–Hf and Sm–Nd isochrons for megacrysts from the Premier (a,b), Monastery (c,d) and Frank Smith (e,f) megacryst suites, calculated using Isoplot (Ludwig, 2003) and a decay constant of 1.865×10^{-11}/a (Scherer *et al.*, 2001). Errors on $^{176}Hf/^{177}Hf$ and $^{143}Nd/^{144}Nd$ ratios are 2SE and taken from Table 2. The $^{176}Lu/^{177}Hf$ and $^{147}Sm/^{144}Nd$ ratios are calculated from ICP-MS elemental data and 2-sigma errors are set at 3%. Closed diamonds are megacryst points, labelled according to phase. Grey squares or rectangles represent the age-corrected kimberlite whole-rock data from Table 1.

Lastly, Hf is an immobile element compared with Sr, especially in non-reactive phases, such as ilmenite and zircon. Hence, even when silicate phases and the host kimberlite are badly weathered, valuable isotopic information can be obtained.

Garnet, diopside and ilmenite megacrysts from Premier yield a Lu–Hf isochron age (Fig. 6a) of 1266 ± 51 Ma (2σ). This age is within error of the 1202 ± 72 Ma U–Pb perovskite age of Kramers & Smith (1983), the 1179 ± 36 Ma Rb–Sr clinopyroxene megacryst isochron of Smith (1983) and of the 1187 ± 63 Ma (recalculated using ISOPLOT) Sm–Nd megacryst isochron age of Jones (1987). The Sm–Nd isochron age for the same three phases used to determine the Lu–Hf age is considerably less precise at 1180 ± 700 Ma (2σ; Fig. 6b). This large uncertainty is due to the diopside megacryst, which was clearly not in Nd isotope equilibrium with the garnet or ilmenite at 1180 Ma and may, for example, have been related to a different parental magma batch. However, combination of our Sm–Nd isotopic data with those of Jones (1987) yields a more precise age of 1192 ± 62 Ma (2σ), in close agreement with the Lu–Hf isochron age.

The precise initial $^{176}Hf/^{177}Hf$ ratio calculated for the Premier parental megacryst magma (0.282094 ± 23; Fig. 6a) is indistinguishable from the initial $^{176}Hf/^{177}Hf$ ratio of the Premier calcite kimberlite (0.282088 ± 10; Table 1).

The Monastery megacryst suite yields a Lu–Hf isochron age of 91 ± 27 Ma (2σ; Fig. 6c) using the three garnets, the four mono-mineralic ilmenites (excluding repeats), an ilmenite from a zircon–ilmenite intergrowth, the diopside and ilmenite from a single intergrowth, a phlogopite and the average parent/daughter ratio and isotopic composition for all zircon megacrysts. Provided that the garnets are included in any isochron, the choice of zircon or ilmenite megacryst phases has little effect on the calculated age or the initial $^{176}Hf/^{177}Hf$ ratio of the megacryst suite. The imprecision in the age is probably due to a combination of the very limited variation in $^{176}Hf/^{177}Hf$ ratio of the phases analysed (only 0.000083 between the most radiogenic garnet and least radiogenic zircon) and the possibility that the phases crystallized from differing magma batches with slightly differing isotopic compositions. The same Monastery megacryst phases yield a Sm–Nd isochron age of 93 ± 25 Ma (2σ), whereas the three garnet megacrysts alone yield an age of 89 ± 15 Ma (Fig. 6d). All the Lu–Hf and Sm–Nd isochron ages are in excellent agreement with both the 90 Ma U–Pb zircon age (Allsop *et al.*, 1989). The initial $^{176}Hf/^{177}Hf$ and $^{143}Nd/^{144}Nd$ ratios calculated for the megacrysts (0.282724 ± 8 and 0.512669 ± 63; Fig. 6c and d), and hence their parental magma, are also in excellent agreement with those calculated for the Monastery kimberlite. For Hf isotopes, the initial Hf isotope composition of the megacryst parent magma or magmas can be precisely estimated from the ilmenite alone, because of the very low Lu/Hf of this phase. An initial $\Delta\varepsilon_{Hf}$ value of −7, calculated for the megacryst suite isochron initial ratios, should lie within the range measured for the Monastery kimberlite. This is the case (Table 1).

Any combination of megacryst phases from the Frank Smith kimberlite produces Lu–Hf and Sm–Nd isochron correlations (Fig. 6e and f) with ages far in excess of the 114 ± 1.8 Ma age of the host kimberlite (Allsop *et al.*, 1989). The scatter of these data on isochron diagrams is manifest in widely varying ε_{Ndi} and ε_{Hfi} values, indicating that either this system did not remain closed during its evolution and/or the megacrysts selected are derived from multiple batches of magma with different initial isotopic compositions (e.g. Bell & Mofokeng, 1998). Larger-magnitude Hf isotope heterogeneity is found in zircons from Orapa (Table 3; Griffin *et al.*, 2000) and in the Jwaneng and Leicester kimberlites (Griffin *et al.*, 2000). Griffin *et al.* attributed the low ε_{Hfi} values (down to −16) of megacryst zircons to reaction of the parental megacryst magma, derived from the convecting mantle, with CLM during fractional crystallization. We view this possibility as very unlikely for two reasons. First, contrary to the predictions of Griffin *et al.* (2000), the great majority of CLM plots well above the mantle Nd–Hf array, at radiogenic ε_{Hf} values (e.g. Simon *et al.*, 2002; Pearson *et al.*, 2003; Fig. 7). Hence, progressive interaction of a megacryst magma with CLM during crystallization should, in fact, produce the opposite effect and yield zircons with increasingly radiogenic Hf. Although some diopsides in garnet lherzolites can have unradiogenic Hf, these have been shown to originate from infiltrating melts associated with kimberlite magmatism (Simon *et al.*, 2003). Secondly, the Hf content of CLM is very low compared with a megacryst magma that is zircon-saturated. Hence, unreasonable amounts of assimilation of lithosphere with a very atypical composition would be required to explain the low ε_{Hfi}.

Although we accept that there is likely to be some interaction between the megacryst magma and lithospheric peridotite during megacryst crystallization (Hops *et al.*, 1992; Smith *et al.*, 1995; Griffin *et al.*, 2000), which may be a source of minor isotopic variation, we prefer to interpret the isotopic heterogeneity of megacrysts from a single locality as resulting from two main causes. Minor heterogeneity (a few epsilon units, e.g. Frank Smith) could result from multiple batches of parental magma (e.g. Gurney *et al.*, 1998), each with slightly different initial isotopic compositions. Major heterogeneity, e.g. Orapa, Jwaneng and Leicester zircon suites, may result from distinct generations of megacryst crystallization, some of which could significantly precede sampling by the host kimberlite. This is clearly the case at Jwaneng, where the zircon megacrysts can be divided into two distinct age populations (Kinny *et al.*, 1989), with correspondingly different Hf isotope compositions. Although there are no U–Pb ages for the Orapa zircons at present (Table 3), their isotopic compositions would be consistent with the low ε_{Hf} zircon populations being related to an earlier phase of kimberlite activity—either a Group II kimberlite event at approximately 120 Ma or a much earlier Group I-related event at approximately 1200 Ma. Initial Hf isotope ratios, calculated at 120 Ma, for the low ε_{Hf} zircon population at Orapa overlap the low ε_{Hf} end of the Group II kimberlites and their megacrysts (Fig. 3b). However, they also have T_{DM} Hf model ages ranging between 1185 and 1277 Ma overlapping the age for the Premier Group I kimberlite (Fig. 6a and b). We note that the ε_{Hfi} values of the Orapa zircons at *c.* 1200 Ma would be approximately 5 to 7 epsilon units more radiogenic than the initial Hf isotopic composition of the Premier kimberlite or megacryst suite (Fig. 6a). Both of these options suggest a genetic link between megacrysts and kimberlite-related magmatism, and work is in progress to determine U–Pb ages of the Orapa zircons, to ascertain whether the low

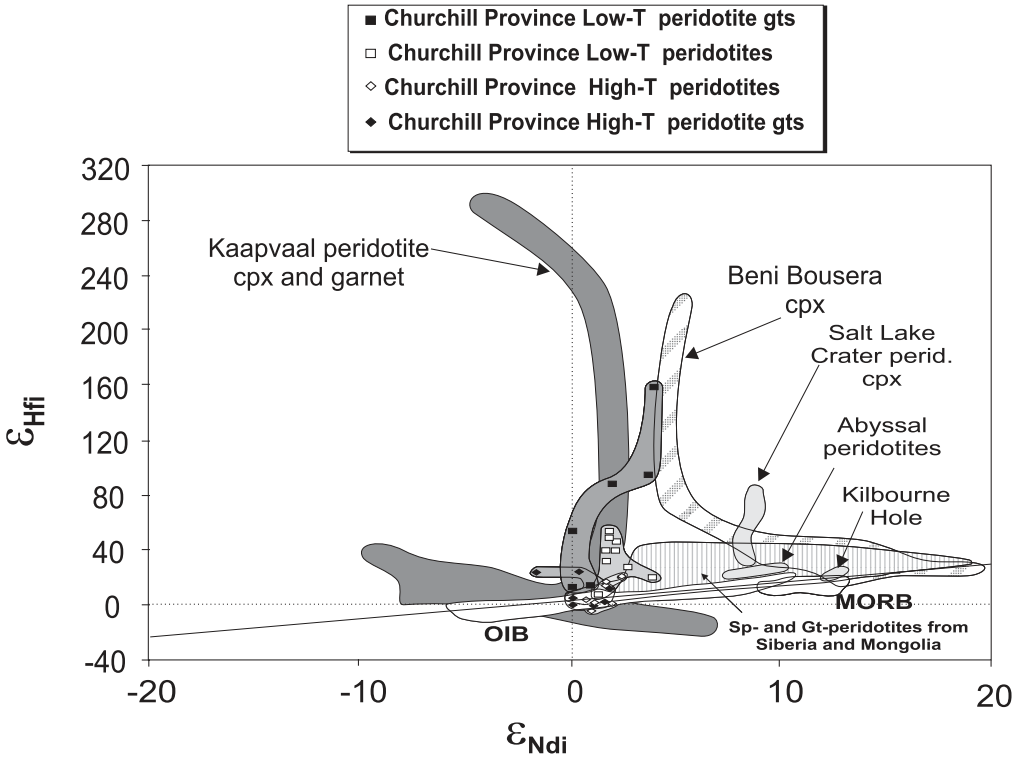

Fig. 7. ε_{Hf}–ε_{Nd} isotope plot for lithospheric mantle peridotite minerals. Kaapvaal peridotite data are all garnets and clinopyroxenes (Simon *et al.*, 2002). Slave peridotite data are garnets and whole-rocks from Schmidberger *et al.* (2002). Salt Lake Crater peridotites (Hawaii), Kilbourne Hole and Abyssal Peridotites are from Salters & Zindler (1995). Siberian and Mongolian peridotite field is for clinopyroxene data from cratonic and off-craton peridotites (Ionov & Weis, 2002). Data sources for MORB (N-MORB) and OIB as in Fig. 1.

ε_{Hf} group is related to an earlier phase of Group I or II kimberlite activity.

Additional support for a link between megacrysts and kimberlites is the close association between the geochemical characteristics of the Cr-poor megacrysts and their kimberlite hosts, together with the systematic differences in trace element geochemistry between megacrysts from Group I and Group II kimberlites. Low-Cr megacrysts from Group I kimberlites have the same isotopic systematics as Group I kimberlites, whereas low-Cr megacrysts from Group II kimberlites have Group II kimberlite isotopic characteristics (Figs 2b, 3b and 5; Bell *et al.*, 1995; Smith *et al.*, 1995).

On the basis of REE data, Harte (1983) suggested that the parental megacryst magma is more similar to alkali basalt produced from the OIB source rather than a kimberlitic liquid. Additional REE data for ilmenites (Nowell & Pearson, 1998, and unpublished) show that their equilibrium liquids can range from those characteristic of OIB magmas to melts significantly more enriched than Group I kimberlites. For instance, for the Monastery kimberlite, La_n and $(La/Dy)_n$ values range from 414 to 485 and 24 to 26, respectively, whereas the calculated equilibrium melt to the ilmenite megacrysts from this kimberlite has La_n 94–2000 and $(La/Dy)_n$ 19–85. Hence, although dependent on the accuracy of partition coefficients, the ilmenites could have been in equilibrium with a kimberlitic melt which may have become LREE enriched and developed high LREE/HREE ratios, as a result of early fractionation of megacryst garnet from a more OIB-like parental magma. A genetic link between kimberlites and their megacrysts is also supported by recent experimental studies that are able to crystallize intergrowths of clinopyroxene plus oxides at high pressures on the liquidus that are exact analogues to the intergrowths found in the low-Cr megacryst suite (Mitchell, 2003).

ORIGIN AND NATURE OF THE NEGATIVE $\Delta\varepsilon_{HF}$ COMPONENT IN KIMBERLITES AND THEIR MEGACRYSTS: EVALUATING THE ROLE OF LITHOSPHERIC MANTLE

Group I kimberlites, Transitional kimberlites and their low-Cr megacrysts are all characterized by negative $\Delta\varepsilon_{Hf}$ signatures of almost exactly the same range (Figs 4 and 5). This relationship was first reported by

Nowell *et al.* (1998*b*, 1999), who proposed that the negative $\Delta\varepsilon_{Hf}$ component was of mantle origin and that it must be ancient in order to deviate significantly from the mantle array. A similar signature is also seen in lamproites (Nowell *et al.*, 1998*a*), although the Hf–Nd isotope systematics of lamproites are distinctly different from kimberlites, despite also being displaced well below the mantle Nd–Hf array (Nowell *et al.*, 2003*b*). Recently, Bizzarro *et al.*, (2002) inferred a negative $\Delta\varepsilon_{Hf}$ signature for the 3 Ga Tupertalik carbonatite from Greenland and concluded that a negative $\Delta\varepsilon_{Hf}$ reservoir, or at least one with unradiogenic ε_{Hfi}, must have been present in the early Earth. However, interpretation of these data is complicated by the fact that the initial Hf isotope composition of the carbonatite is based on a few baddeleyite and zircon analyses whereas the initial Nd isotope composition is based on a single age-corrected whole-rock analysis. The discordant U–Pb systematics of the baddeleyites and zircons clearly indicates that both they and their host carbonatite experienced at least one episode of disturbance following their emplacement at 3 Ga. With an age correction of 3 Ga, even a slight disturbance of the original whole-rock Sm/Nd ratio would result in a significant inaccuracy in the calculated initial whole-rock Nd isotope ratio. Furthermore of the five most concordant baddeleyites and zircons only two have enriched ε_{Hfi} compositions (-3.45 to -4.09) whereas the remaining three have values close to Bulk Earth (-0.03 to 0.47). It is therefore not clear whether the initial isotope composition of the carbonatite was any more enriched than Bulk Earth at 3 Ga or that the enriched ε_{Hfi} compositions reflect post-crystallization disturbance. Given the uncertainty of both the ε_{Hfi} and ε_{Ndi} isotope composition of the Tupertalik carbonatite the significance of a calculated negative $\Delta\varepsilon_{Hf}$ value is unclear and in this work we investigate only the origin of the negative $\Delta\varepsilon_{Hf}$ signature in kimberlites and their megacrysts.

Strikingly negative $\Delta\varepsilon_{Hf}$ signatures were first observed in Southern African kimberlites (Nowell *et al.*, 1999). Recently, the same isotopic characteristics, with $\Delta\varepsilon_{Hf}$ values of equal magnitude, have been found in kimberlites from the Slave Province (Dowall *et al.*, 2000) and Siberia (Nowell & Pearson, unpublished). This signature is not observed to the same extent in any magmas derived from the oceanic convecting mantle, although HIMU OIB have smaller negative $\Delta\varepsilon_{Hf}$ values (Ballentine *et al.*, 1997; Fig. 4b). Janney *et al.* (2002) have recently measured similar, low $\Delta\varepsilon_{Hf}$ isotope compositions in alkaline rocks from Southern Africa and on the continental shelf (Alphard Bank).

The generation of strongly negative $\Delta\varepsilon_{Hf}$ signatures in the kimberlites and other magmatic rocks requires a contribution from a component that has experienced long-term decoupling of Lu/Hf–Sm/Nd systematics. Most mantle-melting processes fractionate Lu/Hf and Sm/Nd in a very systematic way (Fig. 1), as illustrated by the coherence between ε_{Hf} and ε_{Nd} in OIB (Fig. 3; Blichert-Toft *et al.*, 1997; Vervoort *et al.*, 1999). The negative $\Delta\varepsilon_{Hf}$ component requires a larger fractionation of Lu/Hf relative to Sm/Nd than the OIB/MORB source, in order to evolve below the mantle array, i.e. $(f\mathrm{Lu/Hf} > f\mathrm{Sm/Nd})_{\mathrm{kimb\ source}} > (f\mathrm{Lu/Hf} > f\mathrm{Sm/Nd})_{\mathrm{OIB}}$. This component also needs to be isolated from the convecting mantle, to allow its distinctive isotopic signature to evolve and to be preserved (Nowell *et al.*, 1998*b*; Pearson & Nowell, 2002). The component is present in the Premier megacryst suite erupted at 1.2 Ga and, hence, must have been present from early in Earth history. There are several possibilities for the identity and location of this component.

A common factor in the numerous models put forward for the origin of kimberlites is the incorporation of varying amounts of CLM. This ancient reservoir (e.g. Pearson, 1999*a*) is a logical possible location for the negative $\Delta\varepsilon_{Hf}$ component observed in kimberlite magmas because it has remained isolated for billions of years and the occurrence of kimberlites is intimately associated with cratonic CLM (Nowell *et al.*, 1999). Indeed, Griffin *et al.* (2000) argued that CLM was the source of the negative $\Delta\varepsilon_{Hf}$ component initially reported by Nowell *et al.* (1998*b*, 1999). As such, the possibility that this reservoir is the main source contributor to the Nd–Hf isotope systematics of kimberlites should be thoroughly evaluated from both theoretical and observational perspectives.

Theoretical considerations

The major element composition and modal mineralogy of cratonic peridotites indicate that they are the residua of extensive melt extraction (e.g. Boyd, 1989; Pearson *et al.*, 2003). The relative order of partition coefficients for Lu–Hf–Sm–Nd in pyrope (and majoritic) garnet is $D_{Sm} > D_{Nd}$, $D_{Lu} > D_{Hf}$ and $D_{Hf} > D_{Nd}$ (Fig. 1). Hence, extraction of melt within the garnet stability field will lead to residual peridotite compositions that evolve rapidly with time, to radiogenic Hf and Nd isotopic compositions, above the mantle Nd–Hf isotope array and, thus, to highly positive $\Delta\varepsilon_{Hf}$ values (Fig. 8). The complementary melts should evolve to negative $\Delta\varepsilon_{Hf}$ values in the lower left quadrant of Fig. 8. Hence, melt extraction in the presence of garnet and subsequent temporal evolution of residue and melt are an effective way of generating compositions that are distinct from the mantle Nd–Hf isotopic array. Clearly, the highly radiogenic Nd and Hf isotope compositions calculated for evolution of CLM as simple melt residua are not suitable for generating the kimberlite isotopic characteristics, because they evolve to isotopic compositions substantially above the mantle array, with compositions that are not observed in any kimberlite we have measured.

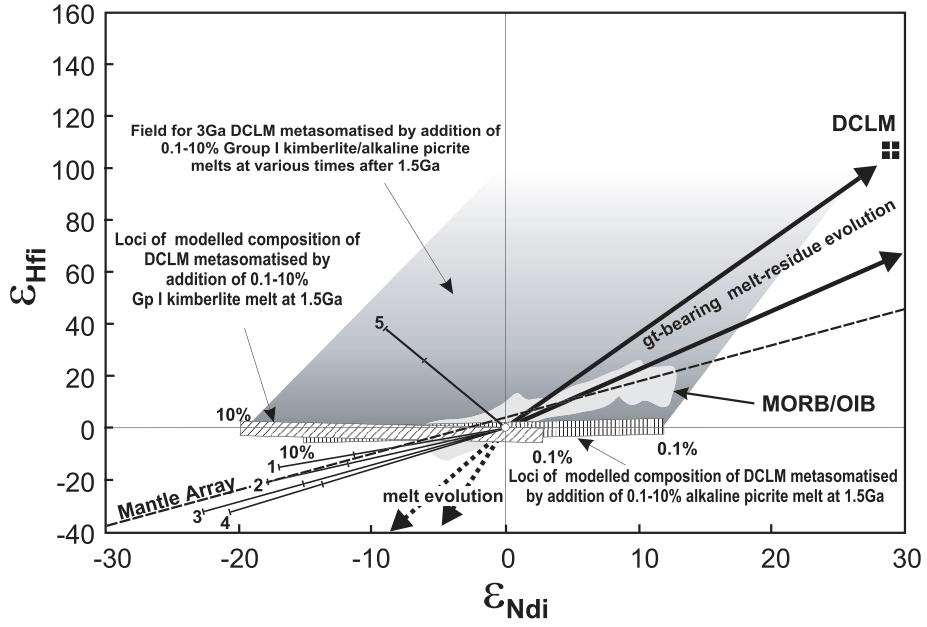

Fig. 8. ε_{Hf}–ε_{Nd} plot showing various theoretical models for the evolution of lithospheric mantle with the mantle array and fields for oceanic basalts (light grey shading), shown for reference. Heavy solid lines extending toward the top right quadrant and Depleted CLM (DCLM) symbol illustrate the isotopic evolution of a melt residue formed by the removal of 10–20% equilibrium melt from a BSE isotopic source in the presence of 10% residual pyrope garnet. [Source mode: olivine: 0.6; orthopyroxene: 0.1; clinopyroxene: 0.2; garnet: 0.1. Melt mode: olivine: 0.1; orthopyroxene: 0.3; clinopyroxene: 0.6; garnet: 0.02. *D* values taken from Blichert-Toft & Albarede (1997)]. The evolution of the complementary melt is shown as dashed lines extending into the lower left quadrant at negative $\Delta\varepsilon_{Hf}$ values. Horizontal bars with diagonal and vertical lines at $\varepsilon_{Hf} \sim 0$ and ε_{Nd} between −20 and 12 represent the present-day modelled composition of depleted CLM (DCLM), formed at 3 Ga and subsequently metasomatized at 1.5 Ga by addition of between 0.1 and 10% of an average Group I kimberlite melt (Smith *et al.*, 1985) or alkaline picrite melt (Mahotkin *et al.*, 2000), respectively. The smaller percentage additions of kimberlite or alkaline picrite are characterized by increasingly radiogenic ε_{Nd} compositions, with the most radiogenic ε_{Nd} values being produced by metasomatism with alkaline picrite. Graded shading shows the region that would be occupied if the metasomatism occurred at times <1.5 Ga and/or the starting DCLM was characterized by more radiogenic ε_{Hf}–ε_{Nd} compositions prior to metasomatism. This field generally encompasses those compositions measured for CLM peridotites (Fig. 7). Vectors labelled 1–5 show the isotopic evolution of various metasomite compositions from an initial starting BSE isotopic composition over 1–1.5 Ga. 1. Average carbonate metasomatized spinel peridotite (Yaxley *et al.*, 1991); 2. AJE281, MARID (Gregoire *et al.*, 2002); 3. AJE18, Phlogopite K-richterite peridotite (Pearson & Nowell, 2002); 4. MARID (Pearson & Nowell, 2002); 5. 22-79 mica pyroxenite (Pearson & Nowell, 2002). Compositions 1–4 evolve to both unradiogenic ε_{Hf} and ε_{Nd} but remain close to the mantle array and, hence, have $\Delta\varepsilon_{Hf}$ values close to zero. The mica pyroxenite (composition 5) rapidly evolves toward unradiogenic ε_{Nd} and very radiogenic ε_{Hf}.

Characterizing ancient CLM as a simple, single-stage melt-residue is unrealistic, given that the petrology and Sr–Nd isotope systematics of lithospheric peridotites indicate significant metasomatic re-enrichment by small-degree melt fractions (e.g. Pearson, 1999*b*). Several models for the isotopic evolution of metasomatized CLM are therefore presented in Fig. 8. This approach is preferable to using the present-day measured parent–daughter ratios of lherzolites and harzburgites, which have often been recently decoupled from their isotopic compositions (Simon *et al.*, 2003) and therefore do not allow accurate prediction of present-day CLM isotopic compositions [e.g. compare the predicted Hf isotopic composition for CLM estimated by Griffin *et al.* (2000, Fig. 5) with the field actually measured; Fig. 7].

The diagonally and vertically ruled bars in Fig. 8 represent the loci of CLM isotopic compositions, calculated at the time of Group I kimberlite eruption at 90 Ma, for a two-stage evolution model. The first stage is depletion of CLM at 3 Ga (DCLM; Fig. 8), and stage two is metasomatism of DCLM at 1.5 Ga by 0.1–10% addition of either average Group I kimberlite (diagonally ruled bar; Smith *et al.*, 1985) or alkaline picrite (vertically ruled bar; Mahotkin *et al.*, 2000), respectively. These metasomatic melts were assigned Bulk Earth ε_{Nd} and ε_{Hf} values at the time of mixing with depleted peridotite and were used because they represent likely metasomatic agents at basal lithospheric levels (200 km).

Addition of small melt fractions to depleted lithospheric peridotite and subsequent storage clearly produce very dramatic changes in isotopic evolution because of the inherently low Nd and Hf contents of highly depleted mantle. In a broad sense, it is difficult to distinguish between metasomatism of DCLM by kimberlite or alkaline picrite melts because they produce very similar results. If metasomatism occurred over a short time interval, then the range in modelled ε_{Hf} at any point (at 90 Ma in Fig. 8) is very limited and relatively independent of the

percentage addition of either kimberlite or alkaline picrite melt. Nd isotopic composition is more sensitive to the mass fraction of added metasomatic melts. Smaller additions in each case result in the evolution of more radiogenic Nd isotope compositions, the alkaline picrite producing slightly more radiogenic ε_{Nd} than the kimberlite. Clearly, the absolute position of the array of mixing trajectories in Fig. 8 is highly sensitive to the selection of the depleted mantle mixing end-member, in terms of both the timing of depletion and metasomatism plus the melting models used to calculate the initial isotopic composition of depleted end-member. For instance, if enrichment of the lithospheric mantle occurred less than 1.5 Ga after the initial melt–depletion event, then it would be possible to generate compositions that evolve to the lower left quadrant, i.e. with negative ε_{Ndi} and ε_{Hfi} and negative $\Delta\varepsilon_{Hf}$ values, similar to values shown by some kimberlites. Equally, if enrichment occurred more recently than 1.5 Ga, it would be increasingly difficult to generate any isotopic compositions suitable as kimberlite source regions.

Despite these caveats, the most notable feature of both models is that the variably metasomatized CLM forms an array oblique to the main mantle array, extending from negative ε_{Nd} and positive $\Delta\varepsilon_{Hf}$ values to positive ε_{Nd} but negative $\Delta\varepsilon_{Hf}$ values (Fig. 8). These trends bear a remarkable similarity to the main trend observed for Kaapvaal peridotites (Fig. 7). The main Kaapvaal peridotite data set cross-cuts the mantle array in a similar manner and at similar ε_{Nd} values to the model predictions (Fig. 8) and has also been attributed to a kimberlite metasomatism process (Simon *et al.*, 2003). The range in ε_{Hf} of the Kaapvaal data is slightly greater than in the kimberlite metasomatism model (diagonally ruled bar; Fig. 8) but it should be remembered that, in the model, initial CLM depletion and subsequent metasomatism occurred at single points in time. Reality is likely to be more complex.

In addition to having suitable isotopic compositions, it is also necessary that kimberlite source regions are incompatible-element enriched and this constraint can be used to further assess the mixing models in Fig. 8. For example, although 0.1% alkali picrite added to depleted mantle at 1.5 Ga and evolved to 90 Ma can produce positive ε_{Ndi} and negative $\Delta\varepsilon_{Hf}$ values, this mixture has <0.2 ppm Nd and <0.05 ppm Hf. These concentrations are far too low to produce the observed Nd and Hf concentrations of a kimberlitic liquid using any melting model. Only when metasomatic melt additions reach upwards of 10% are elemental concentrations in the resulting mix sufficient for the production of even OIB-like melts. At such high added melt fractions, isotopic compositions invariably have positive $\Delta\varepsilon_{Hf}$ values, i.e. unlike Southern African Group I kimberlites.

In addition to this simple modelling, we use the measured Lu/Hf and Sm/Nd of a variety of MARID and amphibole–peridotite (PKP) xenoliths (Gregoire *et al.*, 2002; Pearson & Nowell, 2002) and a mica–pyroxenite (Pearson & Nowell, 2002) to forward model the potential isotopic evolution of solidified vein metasomites and mafic components within the lithosphere. We assume Bulk Earth-like initial isotopic compositions (Fig. 8) for all lithologies. Because MARIDs crystallized recently in the CLM (Hamilton *et al.*, 1998; Konzett *et al.*, 1998), they have not experienced the complex evolution seen by ancient peridotites. For this reason, and because they represent the pure metasome, it is justifiable to use the present-day parent–daughter ratios to forward model their isotopic evolution. The MARID and PKP samples used to model the evolution of vein–metasomatic assemblages have sub-chondritic Sm/Nd and Lu/Hf ratios and so evolve unradiogenic Nd and Hf isotope signatures (i.e. negative ε_{Ndi} and ε_{Hfi}; vectors 2–4, Fig. 8). The isotopic evolution vectors are also sub-parallel to the mantle Hf–Nd array and so, even after 2 Ga of isotopic in-growth, the assemblages remain within error of the mantle array (i.e. $\Delta\varepsilon_{Hf}$ values close to zero). The vectors for MARID assemblages pass through the field of Group II kimberlites, consistent with existing models linking MARIDs to crystallized Group II kimberlites. In contrast to these amphibole-bearing metasomatic assemblages, a mica pyroxenite from the Udachnaya kimberlite (Pearson & Nowell, 2002) has high Lu/Hf but relatively low Sm/Nd, and rapidly evolves to unradiogenic ε_{Nd} and very radiogenic ε_{Hf} compositions, i.e. positive $\Delta\varepsilon_{Hf}$ (vector 5, Fig. 8). Within only a few hundred Ma, the mica pyroxenite evolves outside of the mantle array, as defined by OIB magmas.

Finally, the isotopic evolution of a carbonatite-metasomatized peridotite (Yaxley *et al.*, 1991) is also modelled, although we recognize that this is only one of a potentially large spectrum of carbonatite-metasomatized mantle compositions. The carbonate–peridotite assemblage (vector 1, Fig. 8) also evolves toward unradiogenic Hf and Nd and remains close to the mantle array, even after 2 Ga.

Although the selection of different mixing scenarios may seem somewhat arbitrary and relatively limited, we note that the field for measured CLM (Fig. 7) matches well with the modelled field (Fig. 8) and none of the assemblages modelled evolves to the isotopic characteristics of either Group I kimberlites or their megacrysts.

Direct observations of lithosphere composition and its relationship to kimberlites

Hf isotope analyses have been reported for peridotites from old oceanic lithosphere (Salters & Zindler, 1995). More recently, cratonic (Bedini *et al.*, 2002; Ionov & Weis, 2002; Schmidberger *et al.*, 2002; Simon *et al.*,

2002) and non-cratonic (Blichert-Toft *et al.*, 2000; Ionov & Weis, 2002) CLM peridotites have been analysed, together with garnet pyroxenites and peridotites from the Beni Bousera orogenic massif (Blichert-Toft *et al.*, 1999; Pearson & Nowell, 2003, 2004). This wide spectrum of samples should provide a general picture of the Hf–Nd isotope systematics of lithospheric mantle of various ages.

The database for cratonic CLM (peridotite xenoliths from the Kaapvaal craton and Churchill Province) is dominated by samples that plot close to, or well above, the mantle Nd–Hf array. ε_{Hfi} values are predominantly between 0 and +200 at comparatively unradiogenic ε_{Ndi} values (−20 to +30; Fig. 7; Schmidberger *et al.*, 2002; Simon *et al.*, 2002, 2003, and unpublished). Bedini *et al.* (2002) reported ε_{Hfi} values for Kaapvaal peridotite garnets of up to 2500. Non-cratonic CLM peridotite xenoliths from Siberia and Mongolia (Blichert-Toft *et al.*, 2000; Ionov & Weis, 2002) also plot close to or above the mantle Nd–Hf array, with slightly less extreme ε_{Hfi} values than cratonic peridotites. In addition, peridotite clinopyroxene separates from the Beni Bousera orogenic massif (Pearson & Nowell, 2003) plot on or well above the mantle array with ε_{Hfi} values up to +200 at ε_{Nd} values of between 5 and 20. Overall, the striking feature common to the Kaapvaal, Churchill and Beni Bousera peridotites is the vertical ε_{Hfi}–ε_{Ndi} arrays, with extremely positive $\Delta\varepsilon_{Hf}$ values of some samples (Fig. 7).

The radiogenic Hf isotope compositions observed for metasomatized peridotites and for lithospheric peridotites in general are in keeping with their origin as residua. The radiogenic Hf isotope compositions are not mirrored by the expected radiogenic Nd isotope compositions, which appear to be more disturbed by later metasomatic processes. Ionov & Weiss (2002) concluded that the Hf isotope compositions of some mantle peridotites are much less affected by metasomatism and better preserve the record of ancient depletion events than their Sr or Nd isotope compositions. Although the simple mixing models presented in Fig. 8 are an inadequate representation of the true and complex nature of metasomatism in the mantle, many of the lithospheric peridotites have compositions that fall within the broad fields predicted for melt-metasomatized depleted mantle. As a reservoir, the peridotitic fraction of the CLM is thus characterized by dominantly radiogenic ε_{Hf} at variable ε_{Nd}, placing it substantially above the mantle array in most instances and, hence, being unsuitable as a kimberlite source region. In addition, rocks that represent pure metasomatic rocks do not have Nd–Hf isotope characteristics similar to the Group I and Transitional kimberlites and, hence, we cannot agree with the model of Griffin *et al.* (2000), in which the dominant source for Group I kimberlites is ancient, silicate melt-metasomatized CLM.

Limited data are also available for the mafic components of the CLM, i.e. eclogites and pyroxenites. Pyroxenites from orogenic peridotite massifs represent the effects of melt infiltration into CLM (Blichert-Toft *et al.*, 1999; Pearson & Nowell, 2004). Some samples have unradiogenic Nd and Hf, plotting on the mantle Hf–Nd isotope array. Other samples have very radiogenic Nd isotope compositions, $\varepsilon_{Nd} \sim 35$, but less radiogenic $\varepsilon_{Hf} \sim 20$, such that they plot in the far right quadrant of the diagram, well below the array (Pearson & Nowell, 2004). Cratonic eclogite xenoliths are even more variable, with samples plotting from well below, to well above, the array (Jacob *et al.*, 2002), and Nowell *et al.* (2003*c*) have reported ε_{Hfi} values in South African and Siberian alkremites of between 0 and +24960, with moderately unradiogenic ε_{Ndi} values of between 0 and −10. Some eclogite compositions have very low $\Delta\varepsilon_{Hf}$ values, so that they could be considered as possible sources of the low $\Delta\varepsilon_{Hf}$ signature in kimberlites. One problem with this model is that cratonic eclogites are so isotopically heterogeneous that if they contributed significant Hf to a kimberlite parental melt, we would expect to observe extremely variable Hf and Nd isotope compositions, scattered both above and below the mantle array. In contrast, the kimberlites and their coexisting megacrysts form a systematic, tightly clustered field in Nd–Hf isotope space (Fig. 3b), inconsistent with the incorporation of a highly variable source component such as cratonic eclogite. Furthermore, significant fractions of eclogite should also contribute large amounts of radiogenic Os to the system and this is also inconsistent with the observed OIB-like Os isotope systematics of kimberlites (Pearson *et al.*, 1995, 1996). Even kimberlites that contain abundant eclogite xenoliths (e.g. Roberts Victor) do not show isotopic evidence of having incorporated this lithology into the parental kimberlite magma. Group II kimberlites, which are commonly held to contain the largest lithospheric inputs in any petrogenetic model (Smith, 1983; le Roux, 1986), have Nd–Hf isotope compositions that plot on or above the mantle array.

An additional line of evidence that suggests that ancient cratonic CLM is not the source of the negative $\Delta\varepsilon_{Hf}$ signature in kimberlites comes from the study of alkalic volcanics, erupted around the periphery of the Kaapvaal craton (Janney *et al.*, 2002). Melilitites from the Western Cape Province have Os–Pb signatures that indicate a lithospheric source. These rocks have moderate $\Delta\varepsilon_{Hf}$ values (−4 to −5). With increasing distance away from the craton, where lithosphere becomes progressively thinner, alkali basalts from the Alphard Bank area, located off-shore, have $\Delta\varepsilon_{Hf}$ values as low as −8.3. This appears to reflect the increasing contribution from sub-lithospheric, deeply derived sources (Janney *et al.*, 2002). A similar argument can be made for South African kimberlites, where the lowest $\Delta\varepsilon_{Hf}$ values are found in

Transitional kimberlites, erupted through thinner CLM at the margin of the Kaapvaal craton.

The link between the low-Cr megacryst suite and kimberlites implied above offers a final constraint on the potential involvement of CLM in the genesis of kimberlite-related magmas. Megacrysts from 90 Ma South African Group I kimberlites, excepting the very low ε_{Hfi} Orapa samples, show remarkable Hf isotopic homogeneity (average $\varepsilon_{Hfi} = 0.85 \pm 1.4$; 1 SD). This homogeneity suggests a very widespread (central Botswana–N. Lesotho–Karoo region) megacryst formation event at this time, with the parental melts originating from a laterally widespread and remarkably homogeneous source. Such isotopically homogeneous melts are very unlikely to have originated from, or substantially interacted with, an ancient and isotopically complex source such as CLM.

ORIGIN AND NATURE OF THE NEGATIVE $\Delta\varepsilon_{Hf}$ COMPONENT IN KIMBERLITES AND THEIR MEGACRYSTS: SUBLITHOSPHERIC CONTRIBUTIONS

If the parental kimberlite and megacryst magmas are derived from sublithospheric mantle sources, i.e. the convecting mantle or some deep boundary layer within it, they must contain an isotopic component that is not as clearly recorded in other magmas originating from these reservoirs, e.g. OIB. Although the Southern African kimberlites are only Mesozoic in age, their unradiogenic Hf at relatively radiogenic Nd isotope compositions suggests derivation from a distinctive source that has been isolated from the convecting mantle for considerable periods of time (>1 Gyr). Below, we explore processes that might produce such an isotopically distinctive source.

Fractionation involving perovskite-structured $MgSiO_3$

Perovskite-structured $MgSiO_3$ (hereafter referred to as Mg-perovskite) is a high-pressure mantle phase that has distinctive Lu–Hf and Sm–Nd fractionations (Fig. 1), capable of creating time-integrated negative $\Delta\varepsilon_{Hf}$ signatures (extrapolating the systematics shown in Fig. 1 with time). Either a Mg-perovskite-bearing melt residue (Blichert-Toft & Albarede, 1997) or a Mg-perovskite 'cumulate' from an early terrestrial magma ocean (Salters & White, 1998) will evolve unradiogenic ε_{Hf} and radiogenic ε_{Nd} isotope compositions. Published silicate melt–Mg-perovskite D values for Lu, Hf, Sm and Nd vary greatly (Kato *et al.*, 1988*a*, *b*; Ohtani *et al.*, 1995; Minarik *et al.*, 1998), although the relative ordering of D values derived from any one experiment is always $D_{Sm} > D_{Nd}$, $D_{Hf} > D_{Lu}$, $D_{Hf} > D_{Nd}$ (Fig. 1). Hence, it is possible to model situations involving Mg-perovskite fractionation that could generate isotopic compositions suitable for the negative $\Delta\varepsilon_{Hf}$ component in kimberlites and their megacrysts. However, consideration of whole-Earth Lu–Hf isotope systematics suggests that major Mg-perovskite fractionation did not affect the Early Earth (Blichert-Toft & Albarede, 1997) and this option will not be considered further.

Subducted oceanic crust

Of magmas derived from convecting mantle, those displaying HIMU characteristics show the most pronounced negative $\Delta\varepsilon_{Hf}$ and have relatively radiogenic ε_{Nd} (Chauvel *et al.*, 1994; Ballentine *et al.*, 1997). HIMU basalts are widely accepted to contain a significant fraction of recycled oceanic crust in their source (e.g. Hofmann, 1997). Lu/Hf and Sm/Nd partitioning behaviour during formation of oceanic crust produced by melting in the garnet stability field (Fig. 1), followed by isotopic evolution for >1 Gyr, is capable of generating unradiogenic Hf at a given Nd isotope composition, i.e. negative $\Delta\varepsilon_{Hf}$ characteristics such as those observed in the kimberlite and megacryst source regions (Fig. 9).

It is simple to model the isotopic evolution of subducted MORB. Here, we use measured Sm/Nd and Lu/Hf ratios of modern E- and N-MORB, recognizing that significant uncertainty arises because of the currently unconstrained parent–daughter isotope fractionations during subduction. E-MORB has both sub-chondritic Lu/Hf and Sm/Nd ratios and so evolves unradiogenic ε_{Hf} and ε_{Nd} (Fig. 9). E-MORB also develops negative $\Delta\varepsilon_{Hf}$ values. Ancient E-MORB overlaps the field for Group I kimberlites and extends to the fairly extreme compositions found in the Transitional kimberlites. N-MORB is characterized by sub-chondritic Lu/Hf but supra-chondritic Sm/Nd ratios and so evolves to unradiogenic ε_{Hf} and radiogenic ε_{Nd} with time. Hence, the negative $\Delta\varepsilon_{Hf}$ values at radiogenic ε_{Nd} overlap the field for Group I kimberlites and their megacrysts (Figs 4 and 5), but the ancient N-MORB field does not extend to the compositions of the Transitional kimberlites. Consequently, the component generating the negative $\Delta\varepsilon_{Hf}$ values in the parental kimberlite melts could be a spectrum of subducted, ancient MORB compositions ± a sediment component, stored at a deep boundary layer in the mantle or perhaps trapped in the Transition zone.

Proof that ancient subducted oceanic crustal compositions can evolve to extreme Hf isotopic compositions is seen in the eclogite xenoliths analysed by Jacob *et al.* (2002). The link between kimberlites and ancient

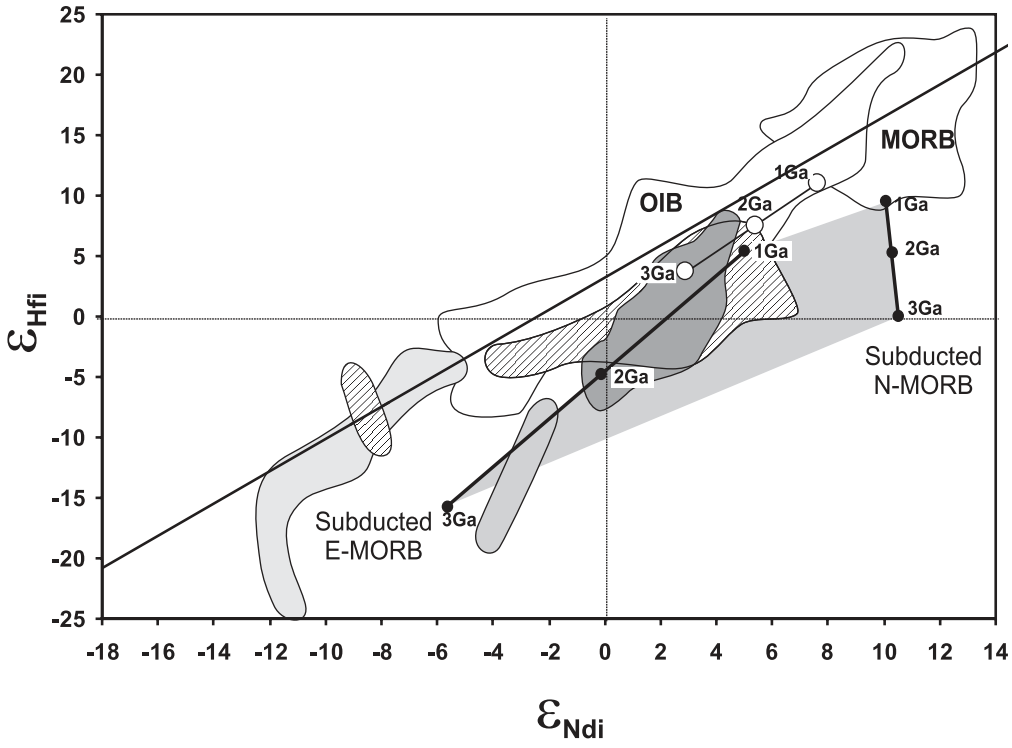

Fig. 9. ε_{Hf}–ε_{Nd} isotope evolution of subducted E-MORB and N-MORB generated at time *t* from a DM source. The isotopic composition of the DM source at time *t* (open circles) is calculated assuming a present-day average $^{176}Hf/^{177}Hf$–$^{143}Nd/^{144}Nd$ DM composition of 0.283200 and 0.513150, respectively, and formation of the DM reservoir from BSE at 4 Ga, giving $^{176}Lu/^{177}Lu$ and $^{147}Sm/^{144}Nd$ ratios of 0.039 and 0.2165, respectively. The isotopic evolution and present-day isotopic compositions of subducted/stored E- and N-MORB generated from a DM source at time *t* are represented by solid lines punctuated with filled circles and are calculated assuming present-day average Lu/Hf and Sm/Nd ratios for E- and N-MORB. Shaded region between E- and N-MORB illustrates possible compositional range between the two extremes and encompasses those compositions observed in the Group I kimberlites (shading as in Figs 1–3) and their associated megacrysts (diagonally hatched shading).

subducted oceanic crust entering their source regions in the deep mantle was first proposed by Sharp (1974) and developed on a geochemical basis by Ringwood (1989). Similarly, Janney *et al.* (2002) have interpreted the low $\Delta\varepsilon_{Hf}$ signatures of melilitites and alkali basalts from Southern Africa as being derived from recycled ancient oceanic crust 'pods' in the asthenosphere.

If the low $\Delta\varepsilon_{Hf}$ component sampled by Group I and Transitional kimberlites is stored in a deep Earth boundary layer, such as the Transition Zone or the core–mantle boundary, it must be entrained during plume-upwelling that ultimately results in kimberlite magmatism (le Roux, 1986; Hops *et al.*, 1992; Haggerty, 1994; Kesson *et al.*, 1994). Os isotopic compositions of Group I and Group II kimberlites show a large degree of overlap, with both groups having a significant population of samples with the same composition as the OIB source. This has led to the suggestion that the ultimate source for both groups of kimberlites is the convecting mantle (Pearson *et al.*, 1995, 1996). In this type of model, the absence of a significant $\Delta\varepsilon_{Hf}$ signature in Group II kimberlites would be a result of extensive hybridization or interaction with lithospheric mantle (characterized by $\Delta\varepsilon_{Hf}$ values of zero to very positive) during kimberlite ascent. Such a model is consistent with the suggestions of Haggerty (1994) and Kesson *et al.* (1994) that the source region for kimberlites is ultra-deep. A deep, sub-lithospheric source region for kimberlites has also received support from phase equilibria studies (Edgar & Charbonneau, 1993; Kesson *et al.*, 1994; Girnis *et al.*, 1995; Mitchell, 2003).

WIDER IMPLICATIONS

Nowell *et al.* (1998*b*, 1999) recognized that the distinctive isotopic signature of kimberlite source regions, i.e. the radiogenic ε_{Nd}, unradiogenic ε_{Hf} component, is relevant to the broader problem of the Hf–Nd isotope composition of Bulk Silicate Earth (BSE), as identified by Blichert-Toft & Albarede (1997). The restricted nature of the mantle Nd–Hf array raises a geochemical mass balance problem in the Earth because the estimates for the Hf–Nd isotope composition of BSE (Blichert-Toft & Albarede, 1997). The Hf/Nd elemental ratios of the

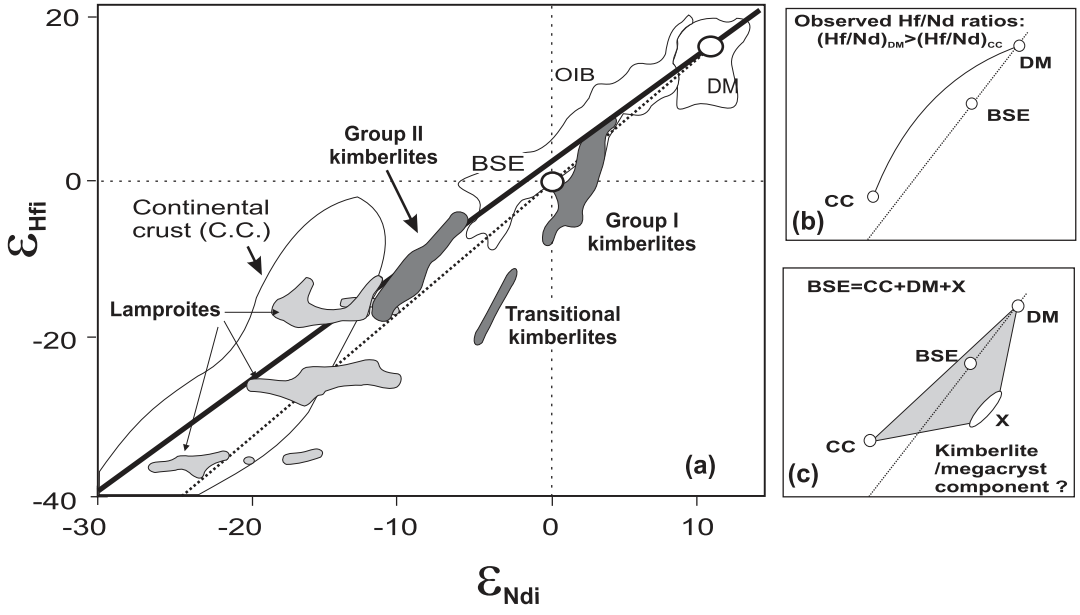

Fig. 10. (a) ε_{Hf} versus ε_{Nd} for modern oceanic basalts and Archaean crustally derived granites adapted from Fig. 3 of Blichert-Toft & Albarede (1997). DM: Depleted Mantle, CC: Continental Crust. Also shown are the fields of Group I, Group II and Transitional kimberlites and lamproites (Table 1; Nowell *et al.*, 2003, and unpublished). (b) Sketch of observed mixing relationship between DM and CC relative to BSE. (c) Modelling of BSE by mass balance between CC, DM and a third component that lies below the mantle array.

Depleted Mantle and Continental Crust reservoirs are such that mixing curves in Hf–Nd isotope space between these two reservoirs do not pass through the Blichert-Toft & Albarede (1997) estimate of BSE (Fig. 10).

Three possible explanations for this apparent mass balance problem have been proposed:

(1) The Earth itself is not chondritic.
(2) The BSE parameters for Hf (and possibly Nd) isotopes defined from meteorites are not a reasonable representation of BSE.
(3) There is a substantial ancient 'hidden reservoir' within the Earth, apparently unsampled by any measured terrestrial volcanic rock, which has a Nd–Hf isotope composition sufficient to compensate for the imbalance between BSE–DM–CC.

When option 3—the 'hidden reservoir'—was first proposed (Blichert-Toft & Albarede, 1997), there was minimal isotopic evidence from terrestrial magmas for its existence. Kimberlites and their megacrysts provided the first identification of mantle-derived magmatic rocks that had isotopic compositions indicative of such a reservoir (Nowell *et al.*, 1998*b*, 1999; Pearson & Nowell, 2002). Trace element and isotopic mass balance constraints show that the location of the proposed missing component is unlikely to be the lithospheric mantle (Rudnick *et al.*, 2000; Pearson & Nowell, 2002). This negative $\Delta\varepsilon_{Hf}$ component is evident in the megacryst suite from the 1.2 Ga Premier kimberlite, indicating that the reservoir must be older. Modelling constraints indicate a likely age of > 2 Ga for this component (Nowell *et al.*, 1999; Fig. 8). The necessity of a substantial 'hidden reservoir' based on mantle Hf–Nd isotope constraints is still the subject of debate (e.g. Allegre, 2002). However, the extremely radiogenic Hf isotopic compositions measured for the residual lithospheric mantle (Fig. 7) require that their complementary melts will evolve to unradiogenic Hf isotope compositions substantially below the array. These solidified melts will be high in Hf, because Hf in the residual lithosphere is very low. If the lithosphere constitutes approximately 2% of BSE (Pearson & Nowell, 2002) and is residual after, on average, 20% melting, then the very negative $\Delta\varepsilon_{Hf}$ reservoir caused by this process alone may constitute in the order of 0.4% of the BSE. In this sense, the highly positive $\Delta\varepsilon_{Hf}$ values of CLM are the strongest argument for the existence of a negative $\Delta\varepsilon_{Hf}$ 'missing' component, irrespective of BSE estimates.

CONCLUSIONS

- Group I and Transitional kimberlites, together with low-Cr megacrysts from Group I kimberlites, have distinctive Hf–Nd isotope systematics that trend below the mantle array at oblique angles and extend significantly outside the field for oceanic basalts, i.e. they have strongly negative $\Delta\varepsilon_{Hf}$ values.

- The matching of kimberlite and megacryst isotopic compositions from each kimberlite group supports a model in which the megacrysts are in some way related to their host kimberlite, or at least share the same source regions.
- Minimally contaminated Group II kimberlites and their low-Cr megacrysts have less radiogenic Hf isotope compositions and plot close to the mantle array, with $\Delta\varepsilon_{Hf}$ values close to zero.
- The presence of megacrystal zircons with Hf isotope compositions substantially less radiogenic than the host kimberlite may be linked to earlier Group I or Group II kimberlite events.
- The continuum of Hf isotope compositions between Group I and II kimberlites is consistent with a model where both groups originate from within the asthenosphere and experience different degrees of hybridization or interaction with enriched lithospheric components.
- The wide range in Lu/Hf shown by phases comprising the low-Cr megacryst suite allows the Lu–Hf isotope system to be used for age determination of the host kimberlite eruption in some instances. A 1266 ± 51 Ma (2σ) Lu–Hf isochron for the Premier megacryst suite is comparable in precision with previous estimates of the eruption age of this kimberlite using other techniques. This finding has important implications for dating highly weathered kimberlites. Care must be taken to analyse a suite of megacrysts that are likely to be co-genetic. Furthermore, the analysis of ilmenite allows precise estimation of the initial Hf isotope ratio of the host kimberlite.
- Development of the unusual, negative $\Delta\varepsilon_{Hf}$ systematics observed in the kimberlite source regions requires time-integrated low Lu/Hf relative to Sm/Nd to evolve for billion year timescales, in a reservoir that has been isolated from the homogenizing effects of mantle convection.
- Hf isotope measurements of lithospheric rocks, together with modelling of lithospheric metasomatism, do not favour the continental lithospheric mantle as the likely location of the negative $\Delta\varepsilon_{Hf}$ source component. Modelling indicates that ancient subducted oceanic crust, residing at a deep Earth boundary layer (Transition Zone or core–mantle boundary), is capable of generating Nd–Hf isotope compositions analogous to those seen in the Group I or Transitional kimberlites and their low-Cr megacrysts. MORB in excess of 2 Ga is the likely candidate. Both E- and N-MORB are required to generate the full spectrum of compositions. Incorporation of some of this component into the melting region of carbonated asthenospheric peridotite produces kimberlitic magmas.
- Prevailing estimates for the Bulk Silicate Earth Hf isotope composition, together with the highly positive $\Delta\varepsilon_{Hf}$ values observed in CLM, can be interpreted as requiring the presence of a 'hidden reservoir' somewhere in the mantle, to complete the terrestrial mass balance. The low $\Delta\varepsilon_{Hf}$ component sampled by kimberlites is the clearest manifestation of such a component observed in mantle rocks.
- Contrary to early observations and beliefs that Nd and Hf isotope variations in terrestrial magmatic rocks showed similar coupling, the new kimberlite and CLM data clearly illustrate that mantle processes can result in extreme decoupling of the Lu–Hf and Sm–Nd systems. It therefore seems unsurprising to us that the estimates for Bulk Silicate Earth might be displaced slightly beneath the terrestrial Nd–Hf isotope array.

ACKNOWLEDGEMENTS

We are grateful to Joe Boyd and Peter Nixon for donating the Frank Smith and PHN 1613 megacrysts, to Patricia Doyle for the Gansfontein zircons, to Nancy Coe for sharing with us isotopic data for the Star kimberlite, and to Dave Dowall for isotopic data for four kimberlites. Dmitri Ionov and Nina Simon generously provided unpublished Nd–Hf isotope data for CLM. We thank Bob Zartman for supplying solutions of Monastery zircons, and Chris Ottley for his assistance with ICP-MS trace element analyses. Jeff Vervoort, Vincent Salters, Janne Blichert-Toft, Nina Simon and Roger Mitchell provided many valuable comments on earlier manifestations of this manuscript, which helped to clarify our ideas. We are grateful to Gareth Davies, who spent considerable editorial effort to improve our focus. This work was funded by NERC grant no. GR3/10094 and HEFCE/NERC JREI grant no. DUPEEQ to D.G.P.

REFERENCES

Allegre, C. J. (2002). The evolution of mantle mixing. *Philosophical Transactions of the Royal Society of London A* **360**, 2411–2431.

Allsop, H., Bristow, J. W., Smith, C. B., Brown, R., Gleadow, A. J. W., Kramers, J. D. & Garvie, O. (1989). A summary of radiometric dating methods applicable to kimberlites and related rocks. In: Ross, J. L. (ed.) *Kimberlites and Related Rocks: Their Composition, Occurrence, Origin and Emplacement. Special Publication of the Geological Society of Australia* **14**, 343–357.

Ballentine, C. J., Lee, D. C. & Halliday, A. N. (1997). Hafnium isotopic studies of the Cameroon line and new Hf paradoxes. *Chemical Geology* **139**, 111–124.

Beard, A. D., Downes, H., Hegner, E. & Sablukov, S. M. (2000). Geochemistry and mineralogy of kimberlites from the Arkhangelsk Region, N.W. Russia: evidence for transitional kimberlite magma types. *Lithos* **51**, 47–73.

Bedini, R. M., Blichert-Toft, J., Boyet, M. & Albarede, F. (2002). Lu–Hf isotope geochemistry of garnet–peridotite xenoliths from the Kaapvaal craton and the thermal regime of the lithosphere. *Geochimica et Cosmochimica Acta* **66** (S1), A61.

Bell, D. R. & Mofokeng, S. (1998). Cr-poor megacrysts from the Frank Smith Mine and the source regions of transitional kimberlites. *Extended Abstracts 7th International Kimberlite Conference, Cape Town*, 64–66.

Bell, D. R., Schulze, D. J., Read, G. H., Mattioli, G. S., Shimizu, N., Moore, R. O. & Gurney, J. J. (1995). Geochemistry of Cr-poor megacrysts from the Lace (Group II) kimberlite, S. Africa. *Extended Abstracts 6th International Kimberlite Conference, Novosibirsk*, 52–53.

Bizzarro, M., Simonetti, A., Stevenson, R. K. & David, J. (2002). Hf isotope evidence for a hidden mantle reservoir. *Geology* **30**, 771–774.

Bizzi, L., Smith, C. B., DeWit, M. C. J., Armstrong, R. & Meyer, H. O. A. (1994). Mesozoic kimberlites and related alkalic rocks in south-western Sao Francisco craton, Brazil: a case for local mantle reservoirs and their interaction. In: Leonardos, O. H. & Meyer, H. O. A. (eds) *Kimberlites, Related Rocks and Mantle Xenoliths*. Brasilia: CPRM, pp. 156–171.

Blichert-Toft, J. (2001). On the Lu–Hf isotope geochemistry of silicate rocks. *Geostandards Newsletter* **25**, 41–56.

Blichert-Toft, J. & Albarede, F. (1997). The Lu–Hf geochemistry of chondrites and the evolution of the crust–mantle system. *Earth and Planetary Science Letters* **148**, 243–258.

Blichert-Toft, J. Chauvel, C. & Albarede, F. (1997). Separation of Hf and Lu for high-precision isotope analysis of rock samples by magnetic sector-multiple collector ICP-MS. *Contributions to Mineralogy and Petrology* **127**, 248–260.

Blichert-Toft, J., Albarede, F. & Kornprobst, J. (1999). Lu–Hf isotope systematics of garnet pyroxenites from Beni Bousera, Morocco: Implications for basalt origin. *Science* **283**, 1303–1306.

Blichert-Toft, J., Ionov, D. A. & Albarede, F. (2000). The nature of the sub-continental lithospheric mantle: Hf isotope evidence from garnet peridotite xenoliths from Siberia. *Journal of Conference Abstracts* **5**, 217.

Boyd, F. R. (1989). Compositional distinction between oceanic and cratonic lithosphere. *Earth and Planetary Science Letters* **96**, 15–26.

Carlson, R. W. & Nowell, G. M. (2001). Olivine-poor sources for mantle-derived magmas: Os and Hf isotopic evidence from potassic magmas of the Colorado Plateau. *Geochemistry, Geophysics, Geosystems* **2**, 2000GC000128.

Carlson, R. W., Esperanca, S. & Svisero, D. P. (1996). Chemical and Os isotopic study of Cretaceous potassic rocks from southern Brazil. *Contributions to Mineralogy and Petrology* **125**, 393–405.

Chauvel, C, & Blichert-Toft, J. (2001). A hafnium isotope and trace element perspective on melting of the depleted mantle. *Earth and Planetary Science Letters* **190**, 137–151.

Chauvel, C., Hofmann, A. W. & Vidal, P. (1994). HIMU-EM: The French Polynesian connection. *Earth and Planetary Science Letters* **110**, 99–119.

Davies, G. R., Spriggs, A. J. & Nixon, P. H. (2001). A non-cognate origin for the Gibeon kimberlite megacryst suite, Namibia: implications for the origin of Namibian kimberlites. *Journal of Petrology* **42**, 159–172.

Dowall, D. P., Nowell, G. M., Pearson, D. G., Kjarsgaard, B. A. & Carlson, J. A. (2000). The nature of kimberlite source regions: a Hf–Nd isotope study of Slave Craton kimberlites. *Journal of Conference Abstracts* **5**(2), 357.

Dowall, D. P., Pearson, D. G. & Nowell, G. M. (2003). Chemical pre-concentration procedures for high-precision analysis of Hf–Nd–Sr isotopes in geological materials by plasma ionisation multi-collector mass spectrometry (PIMMS) techniques. In: Holland, J. G. & Tanner, S. D. (eds) *Plasma Source Mass Spectrometry: Applications and Emerging Technologies*. Cambridge: Royal Society of Chemistry, pp. 321–337.

Edgar, A. D. & Charbonneau, H. E. (1993). Melting experiments on a SiO_2-poor, CaO-rich aphanitic kimberlite from 5–10 GPa and their bearing on sources of kimberlite magmas. *American Mineralogist* **78**, 132–142.

Eggler, D. H., McCallum, M. E. & Smith, C. B. (1979). Megacryst assemblages in kimberlite from northern Colorado and southern Wyoming: petrology, geothermometry–barometry and areal distribution. In: Boyd, F. R. & Meyer, H. O. A. (eds) *Kimberlites, Diatremes and Diamonds: Their Geology, Petrology and Geochemistry*. Washington, DC: American Geophysical Union, pp. 213–226.

Fraser, K. J. & Hawkesworth, C. J. (1992). The petrogenesis of group 2 ultrapotassic kimberlites from Finsch Mine, South Africa. *Lithos* **28**, 327–345.

Girnis, A. V., Brey, G. P. & Ryabchikov, I. D. (1995). Origin of Group 1A kimberlites: fluid-saturated melting experiments at 45–55 kbar. *Earth and Planetary Science Letters* **134**, 283–296.

Gregoire, M., Bell, D. R. & le Roux, A. P. (2002). Trace element geochemistry of phlogopite-rich mafic mantle xenoliths: their classification and their relationship to phlogopite-bearing peridotites and kimberlites revisited. *Contributions to Mineralogy and Petrology* **142**, 603–625.

Griffin, W. L., Pearson, N. J., Belousova, E., Jackson, S. E., van Achterbergh, E., O'Reilly, S. Y. & Shee, S. R. (2000). The Hf isotope composition of cratonic mantle: LAM-MC-ICPMS analysis of zircon megacrysts in kimberlites. *Geochimica et Cosmochimica Acta* **64**, 133–148.

Gurney, J. J., Jacob, W. R. O. & Dawson, J. B. (1979). Megacrysts from the Monastery kimberlite pipe, South Africa. In: Boyd, F. R. & Meyer, H. O. A. (eds) *Kimberlites, Diatremes and Diamonds: Their Geology, Petrology and Geochemistry*. Washington, DC: American Geophysical Union, pp. 222–243.

Gurney, J. J., Moore, R. O. & Bell, D. R. (1998). Mineral associations and compositional evolution of the Monastery kimberlite megacrysts. *Extended Abstracts, 7th International Kimberlite Conference, Cape Town*, pp. 290–292.

Haggerty, S. E. (1994). Superkimberlites: a geodynamic window to the Earth's core. *Earth and Planetary Science Letters* **122**, 57–69.

Hamilton, M. A., Pearson, D. G., Stern, R. A. & Boyd, F. R. (1998). Constraints on MARID petrogenesis: SHRIMP II U–Pb zircon evidence for pre-eruption metasomatism at Kampfersdam. *Extended Abstracts 7th International Kimberlite Conference, Cape Town*, 296–298.

Harte, B. (1983). Mantle peridotites and processes—the kimberlite sample. In: Hawkesworth, C. J. & Norry, M. J. (eds) *Continental Basalts and Mantle Xenoliths*. Nantwich: Shiva, pp. 46–91.

Harte, B. (1999). Lower mantle mineral associations in diamonds from Sao Luiz, Brazil. In: Fei, Y., Bertka, C. M. & Mysen, B. O. (eds) *Mantle Petrology: Field Observations and High Pressure Experimentation Special. Publication of the Geochemical Society* **6**, 57–78.

Harte, B. & Gurney, J. J. (1981). The mode of formation of chromium poor megacryst suites from kimberlites. *Journal of Geology* **89**, 749–753.

Hofmann, A. W. (1997). Mantle geochemistry: the message from oceanic volcanism. *Nature* **385**, 219–229.

Hops, J., Gurney, J. J. & Harte, B. (1992). The Jagersfontein Cr-poor megacryst suite—towards a model for megacryst petrogenesis. *Journal of Volcanology and Geothermal Research* **50**, 143–160.

Ionov, D. A. & Weiss, D. (2002). Hf isotope composition of mantle peridotites: first results and inferences for the age and evolution of the lithospheric mantle. *Abstracts, 4th International Conference on Orogenic Lherzolites and Mantle processes*. Japan: Semani, pp. 56–57.

Jacob, D. E., Bizimis, M. & Salters, V. J. M. (2002). Lu–Hf isotopic systematics of subducted ancient oceanic crust: Roberts Victor eclogites. *Geochimica et Cosmochimica Acta* **66**(S1), A360.

Janney, P. E., le Roex, A. P., Carlson, R. W. & Viljoen, K. S. (2002). A chemical and multi-isotope study of the western Cape olivine

melilitite province, South Africa: implications for the sources of kimberlites and the origin of the HIMU signature in Africa. *Journal of Petrology* **43**, 2339–2370.

Johnson, C. M. & Beard, B. L. (1993). Evidence from hafnium isotopes for ancient sub-oceanic mantle beneath the Rio Grande rift. *Nature* **362**, 441–444.

Jones, R. A. (1987). Strontium and neodymium isotopic and rare earth element evidence for the genesis of megacrysts in kimberlites of southern Africa. In: Nixon, P. H. (ed.) *Mantle Xenoliths*. New York: Wiley, pp. 711–724.

Kato, T., Ringwood, A. E. & Irifune, T. (1988*a*). Constraints on element partition coefficients between $MgSiO_3$ perovskite and liquid determined by direct measurements. *Earth and Planetary Science Letters* **90**, 65–68.

Kato, T., Ringwood, A. E. & Irifune, T. (1988*b*). Experimental determination of element partitioning between silicate perovskites, garnets and liquids: constraints on early differentiation of the mantle. *Earth and Planetary Science Letters* **89**, 123–145.

Kesson, S. E., Ringwood, A. E. & Hibberson, W. O. (1994). Kimberlite melting relations revisited. *Earth and Planetary Science Letters* **121**, 261–262.

Konzett, J., Armstrong, R. A., Sweeney, R. J. & Compston, W. (1998). The timing of MARID metasomatism in the Kaapvaal mantle: an ion probe study of zircons from MARID xenoliths. *Earth and Planetary Science Letters* **160**, 133–145.

Kramers, J. C. & Smith, C. B. (1983). A feasibility study of U–Pb and Pb–Pb dating of kimberlites using groundmass mineral and whole-rock fractions. *Chemical Geology, Isotope Geosciences* **1**, 23–38.

Kramers, J. D., Smith, C. B., Lock, N. P., Harmon, R. S. & Boyd, F. R. (1981). Can kimberlites be generated from an ordinary mantle? *Nature* **291**, 53–56.

le Roux, A. P. (1986). Geochemical correlation between Southern African kimberlites and South Atlantic hot spots. *Nature* **324**, 243–245.

Ludwig, K. R. (2003). *Isoplot 3.0. A geochronological toolkit for Microsoft Excel. Berkeley Geochronology Center Special Publication* **4**.

Mahotkin, I. L., Gibson, S. A., Thompson, R. N., Zhuravlev, D. Z. & Zherdev, P. U. (2000). Late Devonian diamondiferous kimberlite and alkaline picrite (proto-kimberlite?) magmatism in the Arkhangelsk Region, N.W. Russia. *Journal of Petrology* **41**, 201–227.

McDonald, I., DeWit, M. J., Smith, C. B., Bizzi, L. A. & Viljoen, K. S. (1995). The geochemistry of the platinum group elements in Brazilian and southern African kimberlites. *Geochimica et Cosmochimica Acta* **59**, 2883–2903.

Minarik, W. G., Hauri, E. H. & Fei, Y. (1998). Direct determination of trace element partitioning between silicate perovskite and peridotite melt. *EOS (Transactions, American Geophysical Union)* **79**, F1010.

Mitchell, R. H. (1986). *Kimberlites: Mineralogy, Geochemistry and Petrology*. New York: Plenum.

Mitchell, R. H. (1995). *Kimberlite, Orangeites and Related Rocks*. New York: Plenum, 410 pp.

Mitchell, R. H. (2003). Experimental studies at 6–12 GPa of the Ondermatjie hypabyssal kimberlite. *Extended Abstracts of the 8th International Kimberlite Conference, Victoria*, 020.

Moore, A. E. & Lock, N. P. (2001). The origin of mantle-derived megacrysts and sheared peridotites: evidence from kimberlites in the northern Lesotho–Orange Free State (South Africa) and Botswana pipe clusters. *South African Journal of Geology* **104**, 23–38.

Moore R. O., Griffin W. L., Gurney J. J., Ryan C. G., Cousens D. R., Shee S. H. & Suter G. F. (1992). Trace element geochemistry of ilmenite megacrysts from the Monastery kimberlite, South Africa. *Lithos* **29**, 1–16.

Nixon, P. H. & Boyd, F. R. (1973). The discrete nodule association in kimberlites in northern Lesotho. In: Nixon, P. H. (ed.) *Lesotho Kimberlites*. Maseru: Cape and Transvaal, pp. 67–75.

Nowell, G. M. & Parrish, R. (2001). Simultaneous acquisition of isotope compositions and parent/daughter ratios by non-isotope dilution solution-mode plasma ionisation multi-collector mass spectrometry (PIMMS) In: Holland, J. G. & Tanner, S. D. (eds) *Plasma Source mass Spectrometry: The New Millenium. Special Publication of the Royal Society of Chemistry* **267**, 298–310.

Nowell, G. M. & Pearson, D. G. (1998). Hf isotope constraints on the genesis of kimberlitic megacrysts: evidence for a deep mantle component in kimberlites. *Extended Abstracts 7th International Kimberlite Conference, Cape Town*, pp. 634–636.

Nowell, G. M., Pearson, D. G., Irving, A. J. & Turner, S. P. (1998*a*). A Hf isotope study of lamproites: Implications for their origins and relationship to kimberlites. *Extended Abstracts 7th International Kimberlite Conference, Cape Town*, pp. 637–639.

Nowell, G. M., Kempton, P. D. & Pearson, D. G. (1998*b*). Hf isotope systematics of kimberlites: Relevance to terrestrial Hf–Nd systmetics: *Extended Abstracts 7th International Kimberlite Conference, Cape Town*, pp. 628–630.

Nowell, G. M., Kempton, P. D., Noble, S. R., Fitton, J. G., Saunders, A. D., Mahoney, J. J. & Taylor, R. N. (1998*c*). High precision Hf isotope measurements of MORB and OIB by thermal ionisation mass spectrometry: insights into the depleted mantle. *Chemical Geology* **149**, 211–233.

Nowell, G. M., Pearson, D. G., Kempton, P. D., Noble, S. R. & Smith, C.B. (1999). Origins of kimberlites: a Hf isotope perspective. In: Gurney, J. J., Gurney, J. L., Pascoe, M. D. & Richardson, S. H. (eds) *Proceedings 7th International Kimberlite Conference, Cape Town*. Goodwood, S. Africa: National Book Printer, pp. 616–624.

Nowell, G. M., Pearson, D. G., Ottley, C. J., Schweiters, J. & Dowall, D. (2003*a*). Long-term performance characteristics of a plasma ionisation multi-collector mass spectrometer (PIMMS): the ThernoFinnigan Neptune. Plasma Source Mass Spectrometry. In: Holland, J. G. & Tanner, S. D. (eds) *Plasma Source Mass Spectrometry: Applications and Emerging Technologies*. Cambridge: Royal Society of Chemistry, pp. 307–320.

Nowell, G. M., Pearson, D. G. & Irving, A. J. (2003*b*). Lu–Hf and Re–Os systematics of lamproites: constraints on their petrogenesis. *Geophysical Research Abstracts* **5**, 05458.

Nowell, G. M., Pearson, D. G., Jacob, D. J., Spetsius, Z. V., Nixon, P. H. & Haggerty, S. E. (2003*c*). The origin of alkremites and related rocks: a Lu–Hf, Rb–Sr and Sm–Nd isotope study. *Extended Abstracts 8th International Kimberlite Conference*, Victoria, FLA 0271.

Ohtani, E., Yurimoto, H., Sagawa, T. & Kato, T. (1995). Element partitioning between Mg–SiO_3 perovskite, magma, and molten iron: constraints for the earliest processes of the Earth–Moon system. In: Yakutaki, T. (ed.) *The Earth's Central Part: Its Structure and Dynamics*. Tokyo: Terra Scientific Publishing Company, pp. 287–300.

Ottley, C. J., Pearson, D. G. & Irvine, G. J. (2003). A routine method for the dissolution of geological samples for the analysis of REE and trace elements via ICP-MS. In: Holland, J. G. & Tanner, S. D. (eds) *Plasma Source Mass Spectrometry: Applications and Emerging Technologies*. Cambridge: Royal Society of Chemistry, pp. 221–230.

Pearson, D. G. (1999*a*). The age of continental roots. *Lithos* **48**, 171–194.

Pearson, D. G. (1999*b*). Evolution of cratonic lithospheric mantle: an isotopic perspective. In: Fei, Y., Bertka, C. M. & Mysen, B. O. (eds) *Mantle Petrology: Field Observations and High Pressure Experimentation Special Publication of the Geochemical Society* **6**, 57–78.

Pearson, D. G. & Nowell, G. M. (2002). The continental lithospheric mantle: characteristics and significance as a mantle reservoir. *Philosophical Transactions of the Royal Society of London A* **360**, 2383–2410.

Pearson, D. G. & Nowell, G. M. (2003). Dating mantle differentiation: a comparison of the Lu–Hf, Re–Os and Sm–Nd isotope systems in the Beni Bousera peridotite massif and constraints on the Nd–Hf composition of the lithospheric mantle. *Geophysical Research Abstracts* **5**, 05430.

Pearson, D. G. & Nowell, G. M. (2004). Re–Os and Lu–Hf isotope constraints on the origin and age of pyroxenites from the Beni Bousera peridotite massif: implications for mixed peridotite–pyroxenite mantle sources. *Journal of Petrology* **45**, 439–455.

Pearson, D. G., Rogers, N. W., Irving, A. J., Smith, C. B. & Hawkesworth, C. J. (1995). Source regions of kimberlites and lamproites: constraints from Re–Os isotopes. *Extended Abstracts, 6th International Kimberlite Conference, Novosibirsk*, 430–432.

Pearson, D. G., Rogers, N. W., Irving, A. J., Smith, C. B. & Hawkesworth, C. J. (1996). Re–Os isotope constraints on the sources of kimberlites and lamproites. *Journal of Conference Abstracts* **1**, 453.

Pearson, D. G., Canil, D. & Shirey, S. B. (2003). Mantle samples included in volcanic rocks: xenoliths and diamonds. In: Turekian, K. K. & Holland, H. D. (eds) *Treatise on Geochemistry, Volume 2: The Mantle and Core*, Amsterdam: Elsevier.

Ringwood, A. E. (1989). Slab–mantle interactions: 3. Petrogenesis of intraplate magmas and structure of the upper mantle. *Chemical Geology* **82**, 187–207.

Royse, K. R., Kempton, P. D. & Darbyshire, D. P. F. (1998). Procedure for the analysis for rubidium–strontium and samarium–neodymium isotopes at the NERC Isotope Geosciences Laboratory. *NERC Isotope Geosciences Laboratory Report Series* **121**, 28 pp.

Rudnick, R. L., Barth, M. G., Horn, I. & McDonough, W. F. (2000). Rutile-bearing refractory ecologites; missing link between continents and depleted mantle. *Science* **287**, 278–281.

Salters, V. J. & White, W. M. (1998). Hafnium isotope constraints on mantle evolution. *Chemical Geology* **145**, 447–460.

Salters, V. J. M. & Zindler, A. (1995). Extreme $^{176}Hf/^{177}Hf$ in the sub-oceanic mantle. *Earth and Planetary Science Letters* **129**, 13–30.

Scherer, E., Munker, C. and Mezger, K. (2001). Calibration of the lutetium–hafnium clock. *Science* **293**, 683–687.

Schmidberger, S. S., Simonetti, A. & Francis, D. (2002). Probing Archean lithosphere using the Lu–Hf systematics of peridotite xenoliths from Somerset Island kimberlites, Canada. *Earth and Planetary Science Letters* **197**, 245–259.

Sharp, W. E. (1974). A plate tectonic origin for diamond-bearing kimberlites. *Earth and Planetary Science Letters* **21**, 351–354.

Simon, N. S. C., Carlson, R. W., Pearson, D. G. & Davies, G. R. (2002). The Lu–Hf isotope composition of cratonic lithosphere: disequilibrium between garnet and clinopyroxene in kimberlite xenoliths. *Geochimica et Cosmochimica Acta* **66** (S1), A717.

Simon, N. S. C., Irvine, G. J., Davies, G. R., Pearson, D. G. & Carlson, R. W. (2003). The origin of garnet and clinopyroxene in 'depleted' Kaapvaal peridotites. *Lithos* **71**, 289–322.

Skinner, E. M. W., Smith, C. B., Viljoen, K. S. & Clarke, T. C. (1994). The petrography, tectonic setting and emplacement ages of kimberlites in the South western Border Region of the Kaapvaal Craton, Prieska area, South Africa. In: Leonardos, O. H. & Meyer, H. O. A. (eds) *Kimberlites, Related Rocks and Mantle Xenoliths*. Brasilia: CPRM, pp. 80–95.

Smith, C. B. (1983). Pb–Sr and Nd isotopic evidence for sources of southern African Cretaceous kimberlites. *Nature* **304**, 51–54.

Smith, C. B., Gurney, J. J., Skinner, E. M. W., Clement, C. R. & Ebrahim, N. (1985). Geochemical character of southern African kimberlites: a new approach based on isotopic constraints. *Transactions of the Geological Society of South Africa* **88**, 267–280.

Smith, C. B., Schulze, D. J., Bell, D. R. & Viljoen, K. S. (1995). Bearing of the subcalcic Cr-poor megacryst suite on kimberlite petrogenesis and lithospheric structure. *Extended Abstracts, 6th International Kimberlite Conference, Novosibirsk*, 546–548.

Spriggs, A. J. (1988). A geochemical and isotopic study of kimberlites from Namibia. Ph.D. thesis, University of Leeds.

Thirlwall, M. (1991). Long-term reproducibility of multicollector Sr and Nd isotope ratio analysis. *Chemical Geology* **94**, 85–104.

Vervoort, J., Patchett, P. J., Blichert-Toft, J. & Albarede, F. (1999). Relationships between Lu–Hf and Sm–Nd isotopic systems in the global sedimentary system. *Earth and Planetary Science Letters* **168**, 79–99.

Wiedenbeck, M., Alle, P., Corfu, F., Griffin, W. L., Meier, M., Oberli, F., Quadt, A. V., Roddick, J. C. & Spiegel, W. (1995). Three natural zircon standards for U–Th–Pb, Lu–Hf, trace element and REE analyses. *Geostandards Newsletter* **19**, 1–23.

Yaxley, G. M., Crawford, A. J. & Green, D. H. (1991). Evidence for carbonatite metasomatism in spinel peridotite xenoliths from western Victoria, Australia. *Earth and Planetary Science Letters* **107**, 305–317.